

Underwater Image Enhancement by Attenuated Color Channel Correction and Detail Preserved Contrast Enhancement

Weidong Zhang[✉], Graduate Student Member, IEEE, Yudong Wang, and Chongyi Li[✉]

Abstract—An underwater image often suffers from quality degradation issues, such as color deviations, low contrast, and blurred details, due to the absorption and scattering of light. In this article, we propose to address the aforementioned degradation issues via attenuated color channel correction and detail preserved contrast enhancement. Concretely, we first propose an underwater image color correction method. Considering the differences between superior and inferior color channels of an underwater image, the inferior color channels are compensated via especially designed attenuation matrices. We then employ a dual-histogram-based iterative threshold method and a limited histogram method with Rayleigh distribution to improve the global and local contrast of the color-corrected image, thus achieving a global contrast-enhanced version and a local contrast-enhanced version, respectively. To integrate the complementary merits between the global contrast-enhanced version and the local contrast-enhanced version, we adopt a multiscale fusion strategy to fuse them. Finally, we propose a multiscale unsharp masking strategy to further sharpen the fused image for better visual quality. Extensive experiments on four underwater image enhancement benchmark data sets demonstrate that our method effectively enhances underwater images qualitatively and quantitatively. Besides, our method also generalizes well to the enhancement of low-light images and hazy images.

Index Terms—Color correction, contrast enhancement, underwater image enhancement, underwater imaging.

I. INTRODUCTION

RECENTLY, underwater imaging has played a vital role in underwater vehicles, inspection of underwater infrastructures, and deep ocean exploration [1]–[5]. Hence, high-quality

Manuscript received September 11, 2020; revised April 18, 2021, July 23, 2021, and October 4, 2021; accepted December 17, 2021. Date of publication March 29, 2022; date of current version July 13, 2022. This work was supported in part by the China Postdoctoral Science Foundation under Grant 2019M660438 and in part by CAAI–Huawei MindSpore Open Fund. (*Corresponding author: Chongyi Li*.)

Associate Editor: H. Zheng.

Weidong Zhang is with the School of Information Engineering, Henan Institute of Science and Technology, Xinxiang 453600, China, and also with the School of Information Science and Technology, Dalian Maritime University, Dalian 116026, China (e-mail: 1021256331@qq.com).

Yudong Wang is with the School of Electrical and Information Engineering, Tianjin University, Tianjin 300072, China (e-mail: yudongwang1226@gmail.com).

Chongyi Li is with the Department of Computer Science and Engineering, Nanyang Technological University, Singapore 639798 (e-mail: chongyi.li@ntu.edu.sg).

The code is publicly available at https://github.com/Li-Chongyi JOE2021_ACDC.

Digital Object Identifier 10.1109/JOE.2022.3140563

underwater images are highly desired for many practical applications. Typically, underwater images suffer from color deviations, low contrast, and blurred details [6], [7]. Two major factors result in the degradation of underwater images. On the one hand, the light reflected from the underwater scene is scattered and absorbed by plankton or suspended particles in the underwater medium before reaching the camera, which leads to the reduced contrast and blurred appearance [8], [9]. On the other hand, the selected attenuation of light with different wavelengths results in color deviations of underwater images [10], [11]. Therefore, how to improve the visual quality of underwater images is a challenging task.

To improve the visual quality of underwater images, the existing methods range from supplementary-information-based, restoration-based, and enhancement-based to deep-learning-based methods [12]. Supplementary-information-based methods [13]–[20] require extra information, whereas restoration-based methods [21]–[34] depend on underwater imaging physical models. However, extra information and complicated physical models and optical factors limit the practical application of these two kinds of method. In addition, deep-learning-based methods [35]–[42] are limited by insufficient or unrealistic training data [43], [44]. Enhancement-based methods [45]–[55] can enhance underwater images without considering underwater imaging physical models and using a mass of training data.

In our study, we follow enhancement-based methods to deal with the quality degradation of underwater images. Inspired by multiscale fusion (MSF) [51], [52], we propose an attenuated color channel correction (ACCC) and detail preserved contrast enhancement method to obtain high-quality underwater images. Specifically, we first produce the color-corrected image from a given underwater image by an ACCC method. Then, we obtain the global and local contrast-enhanced versions from the color-corrected image by a dual-histogram-based iterative threshold method and a limited histogram method with Rayleigh distribution, respectively. MSF technology is employed to combine the advantages of the global and local contrast-enhanced images. Unlike previous fusion-based methods, we only employ the brightness weight map of the luminance channel in the CIELAB color space and the saliency weight map of the combination of hue, saturation, and value channels in the HSV color space as the inputs of the normalized weight map. Finally, we propose a multiscale unsharp masking (MSUM) strategy to further sharpen the edges and details of the result.



Fig. 1. Sample results of our method. Top: quality-degraded images. From left to right are an underwater image sampled from UIEB data set [43], an underwater image sampled from UCSS data set [56], an underwater image sampled from OceanDark data set [57], a low-light image sampled from the Internet, and a hazy image sampled from the Internet. Bottom: the corresponding results enhanced by our method. For different kinds of quality-degraded image, our method does not require any fine-tuning.

Unlike restoration-based and deep-learning-based methods, our method does not require any supplementary information, prior knowledge, and training data. In comparison to previous fusion-based methods [51], [52], our method not only reduces the weight maps without compromising the quality of fusion, but also fully integrates the complementary advantages of the global and local contrast-enhanced versions. Experiments on four underwater image enhancement benchmark data sets (UIEB [43], EUVP [42] UCCS [56], and OceanDark [57]) demonstrate the robustness and effectiveness of our method. Notably, our method is also suitable for enhancing low-light images and hazy images. Fig. 1 presents the results enhanced by our method for various types of quality-degraded image.

The contributions of this article are emphasized as follows.

- 1) We propose an underwater image enhancement method that does not rely on prior information and specialized hardware devices. The proposed method effectively solves the issues of color distortions and low contrast of underwater images.
- 2) We propose an ACCC method, in which the inferior color channels are compensated based on attenuation matrices that are calculated by considering the differences between superior and inferior color channels at each pixel.
- 3) We propose a dual-histogram-based iterative threshold method to improve global contrast and a limited histogram method with Rayleigh distribution to improve local contrast. We found that the combination can effectively improve the contrast of underwater images.
- 4) We propose an MSUM method that further sharpens underwater images.

II. RELATED WORK

Numerous methods have been proposed to improve the quality of underwater images and can be divided into four categories: supplementary-information-based methods, restoration-based methods, enhancement-based methods, and deep-learning-based methods.

A. Supplementary-Information-Based Methods

In the early stage, the supplementary information, including multiple images [13]–[15] and dedicated hardware (e.g., polarization filtering [16], descattering imaging [17], free-ascending deep-sea tripods [18], range-gated imaging [19], and exposure-bracketing imaging [20]), was used to improve the visibility of underwater images. Unfortunately, these supplementary-information-based methods are complex and expensive due to the use of multiple images or specialized hardware devices. Therefore, these factors limit their applications.

B. Restoration-Based Methods

In comparison to the supplementary-information-based methods, single underwater image restoration has been demonstrated to be more suitable for challenging underwater environments, thus attracting more and more attention. Restoration-based methods usually regard the process of image restoration as an ill-posed inverse problem. Some researchers [21] employed the Jaffe–McGlamery model to improve the visibility of underwater images. Akkaynak and Treibitz [22] revised the Jaffe–McGlamery model. The dark channel prior (DCP) [23] was initially proposed to remove fog from outdoor images. Chiang and Chen [24] proposed a systematic underwater restoration method based on the DCP, which improves the quality of underwater images by wavelength compensation and dehazing. Draws *et al.* [25] designed an underwater dark channel prior (UDCP) to estimate the transmission of underwater scenes. The transmission indicates the percentage of the scene radiance reaching the camera, which is a key component of an underwater imaging model. Li *et al.* [26], [27] combined the minimum information loss and histogram distribution prior (MLHP) for underwater image restoration. Peng and Cosman [28] employed image blurriness and light absorption (IBLA) to estimate the underwater scene depth. Li *et al.* [29] proposed a random forest regression model (RFEM) to estimate underwater scene transmission. A generalized dark channel prior (GDCP) method was proposed by Peng *et al.* [30], which introduces an adaptive color-correction method into the underwater image formation model.

Dai *et al.* [31] employed the decomposing curves of attenuating color to restore underwater images. Yang *et al.* [32] employed the reflection-decomposition-based transmission map estimation for offshore underwater image restoration. Recently, the color-lines prior [33] and haze-lines prior [34] were employed for underwater image restoration. In general, the restoration-based methods are sensitive to assumptions and model parameters.

C. Enhancement-Based Methods

Enhancement-based methods obtain the images with better visual quality by modifying image pixel values without considering image formation models. The histogram-based [45]–[47], Retinex-based [48]–[50], and fusion-based methods [51]–[53] have been applied to underwater image enhancement. Ghani and Isa [45] proposed an integrated color model with Rayleigh distribution to improve the contrast and reduce noise of underwater images. Ghani and Isa [46] proposed a dual-image Rayleigh-stretched CLAHE to improve the quality of underwater images. Ghani *et al.* [47] modified the works of [45] and [46] to obtain underwater images with high visibility using recursive-overlapped CLAHE and dual-image wavelet fusion. Fu *et al.* [48] proposed a Retinex-based method to enhance underwater images, which includes color correction, layer decomposition, and contrast enhancement. Zhang *et al.* [49] proposed an underwater image enhancement method based on extended multiscale Retinex, which utilizes the combination of a bilateral filter and a trilateral filter. Zhang *et al.* [50] proposed a multichannel convolutional multiscale Retinex with color restoration to improve the visibility of underwater images. Ancuti *et al.* [51] employed a fusion method to enhance underwater images and videos. Ancuti *et al.* [52] modified the work of [51] to enhance underwater images by color balance and fusion (CBAF). Zhang *et al.* [54], [55] used the fusion of foreground- and background-stretched images to enhance underwater images. In general, the results enhanced by the aforementioned enhancement-based methods tend to produce overenhanced and underenhanced regions.

D. Deep-Learning-Based Methods

The success of a deep learning strategy inspires its application in underwater image enhancement [58]–[65]. Recently, Li *et al.* [35] have proposed an unsupervised generative network for the color correction of monocular underwater images, called WaterGAN. Chen *et al.* [36] proposed a GAN-based underwater image restoration scheme, in which the adversarial loss, underwater index loss, and DCP loss are used. In [37], a multiscale dense generative adversarial network was proposed for underwater image enhancement. Lu *et al.* [38] employed deep convolutional neural networks to address the problem of descattering from low-illumination underwater images. Li *et al.* [39] proposed an underwater image enhancement convolutional neural network model based on underwater scene prior, which uses ten types of synthesized underwater image for training. Yang *et al.* [40] proposed a conditional generative adversarial network for underwater image enhancement. Fu and Cao [41] combined the global-local networks and compressed-histogram equalization

to enhance underwater images and videos. Islam *et al.* [42] proposed a fast underwater image enhancement model. This model can improve the accuracy of underwater target detection. All in all, the results generated by these deep-learning-based methods may bring an unnatural visual appearance. Additionally, deep underwater image enhancement models are limited by the lacking of diverse and high-quality training data.

III. PROPOSED METHOD

The flowchart of our method is shown in Fig. 2. Our method involves the following four steps: 1) ACCC; 2) global and local contrast improvement; 3) MSF; and 4) MSUM. To be specific, the first step is to correct the color casts caused by the selective absorption of light. The second step is introduced to obtain a global contrast-improved image and a local contrast-improved image from the color-corrected image. The third step is employed to integrate the complementary advantages of the global and local contrast-improved versions by an MSF strategy. Finally, the MSUM strategy is applied to the fused image for better visual quality. We will elaborate on the details of our method.

A. Attenuated Color Channel Correction

For turbid water, the green channel is relatively well preserved when compared to the red and blue ones. In this case, we treat the green channel as the superior color channel and use it to compensate the inferior channels (i.e., the red and blue channels). In addition, for a deep-water environment, the blue channel is relatively well preserved. In this case, the blue channel is treated as the superior color channel for compensating the red and green channels. Mathematically, we compute the mean of total pixel intensity values to distinguish these two cases. Specifically, the mean pixel values of each color channel are calculated as

$$\text{Mean}_c = \frac{1}{MN} \sum_{i=1}^M \sum_{j=1}^N I_c(i, j), \quad c \in \{R, G, B\} \quad (1)$$

where M and N are the height and width of the input image I , respectively. The color channel with the maximum mean value is identified as the superior color channel I_{\max} . Subsequently, the other color channels with the intermediate and minimum values are identified as the inferior color channels I_{int} and I_{\min} , respectively.

For degraded underwater images, it should add appropriate pixel intensity values to compensate for the inferior color channels. In brief, the smaller the differences between the superior and inferior color channels is, the better the inferior color channel is compensated and *vice versa* [52], [66]. Consequently, the attenuation matrices Att_{int} and Att_{\min} are determined to compensate for the attenuation of the inferior channels at each pixel. The attenuation matrix Att_{int} is computed by considering the differences between the maximum and intermediate color channels, while the attenuation matrix Att_{\min} is computed by considering the differences between the maximum and minimum color channels. Mathematically, the attenuation matrices

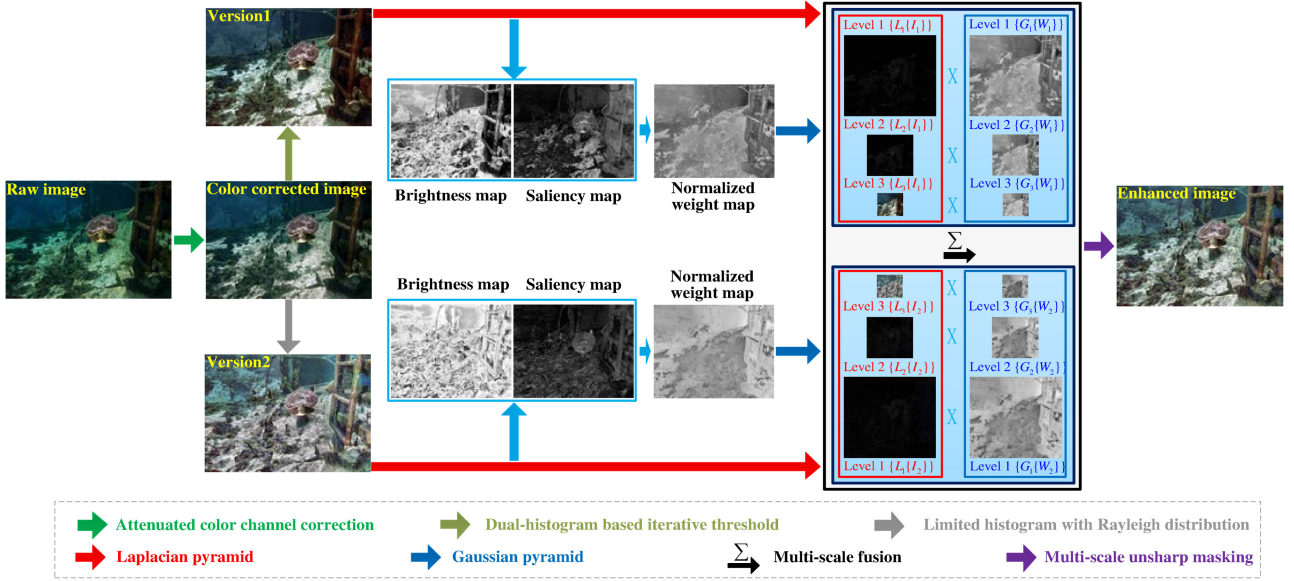


Fig. 2. Overview of our proposed method. Given an underwater image (denoted as Raw image), it is first forwarded to the proposed color correction method. Then, two images, denoted as Version1 (global contrast-improved image) and Version2 (local contrast-improved image), are derived from the color-corrected image by using dual-histogram-based iterative threshold method and limited histogram method with Rayleigh distribution, respectively. Version1 and Version2 are then as inputs of the fusion stage to compute the normalized weight maps that are used to integrate the inputs based on an MSF with three levels of Laplacian and Gaussian pyramids. Finally, our MSUM is used to sharpen the fused image, thus achieving the final result (denoted as Enhanced image).

Att_{int} and Att_{min} are calculated by

$$\text{Att}_{\text{int}}(i, j) = I_{\max}(i, j) - I_{\text{int}}(i, j) \quad (2)$$

$$\text{Att}_{\text{min}}(i, j) = I_{\max}(i, j) - I_{\min}(i, j) \quad (3)$$

where $I_{\max}(i, j)$, $I_{\text{int}}(i, j)$, and $I_{\min}(i, j)$ are the pixel values of the superior, intermediate, and inferior color channels at position (i, j) , respectively. After the attenuation matrices Att_{int} and Att_{min} are determined, the inferior color channels are compensated by

$$I_{\text{int}}(i, j) = I_{\text{int}}(i, j) + (\text{Att}_{\text{int}}(i, j) \times I_{\max}(i, j)) \quad (4)$$

$$I_{\min}(i, j) = I_{\min}(i, j) + (\text{Att}_{\text{min}}(i, j) \times I_{\max}(i, j)). \quad (5)$$

Furthermore, a simple yet effective linear stretch, as defined in (6), is applied to each compensated color channel so that all pixels of each color channel cover the entire dynamic range of the image

$$I_{\text{CR}} = O_{\min} + (I_{\text{in}} - I_{\text{low}}) \times \left(\frac{O_{\max} - O_{\min}}{I_{\text{high}} - I_{\text{low}}} \right) \quad (6)$$

where I_{in} is the color compensated image, I_{CR} is the corrected result, and $I_{\text{in}} \in \{I_{\max}, I_{\text{int}}, I_{\min}\}$. O_{\min} and O_{\max} are the minimum and maximum values of the output image, respectively, and I_{low} and I_{high} are the minimum and maximum values of the color compensated image, respectively.

Fig. 3 shows the color-corrected results of our method. Fig. 3(a) shows a sample where the green channel outperforms the red and blue channels. In Fig. 3(b), the proposed color-correction method significantly reduces the unwanted green distortion, while the histogram distributions of the three channels are more uniform and similar. In contrast, Fig. 3(c) shows a degraded underwater image captured in the deep underwater

environment. In Fig. 3(d), the proposed method also significantly reduces the unwanted blue distortion, while the histogram distributions of the three channels are more uniform and similar. Additionally, observing Fig. 3(b) and (d), we can see that the mean value of each color channel is close.

Despite the good performance of our color-correction method for reducing the color casts of underwater images, using this step alone is insufficient to handle the degraded visibility of underwater images. This is because the details and edges of underwater images are deteriorated by the scattering. Thus, we apply a dual-histogram-based iterative threshold method and a limited histogram method with Rayleigh distribution to improve the global and local contrast of the underwater image, respectively.

B. Global and Local Contrast Improvement

The main purpose of this step is to improve the contrast of underwater images. Specifically, a dual-histogram-based iterative threshold method is used to improve the global contrast, while a limited histogram method with Rayleigh distribution is used to improve the local contrast. We detail them as follows.

1) *Dual-Histogram-Based Iterative Threshold*: Recently, the mean point [45], median point [46], and average point of the mean and median [67] were applied to divide the histogram into two regions. However, these methods simply divide the histogram into two regions and do not sufficiently consider dividing the image into background and foreground subimages. Unlike these methods, we observed the fact that most captured underwater images have dark regions in the background and bright regions in the foreground. Precisely, the regions near the light source are brighter than the region far away from the

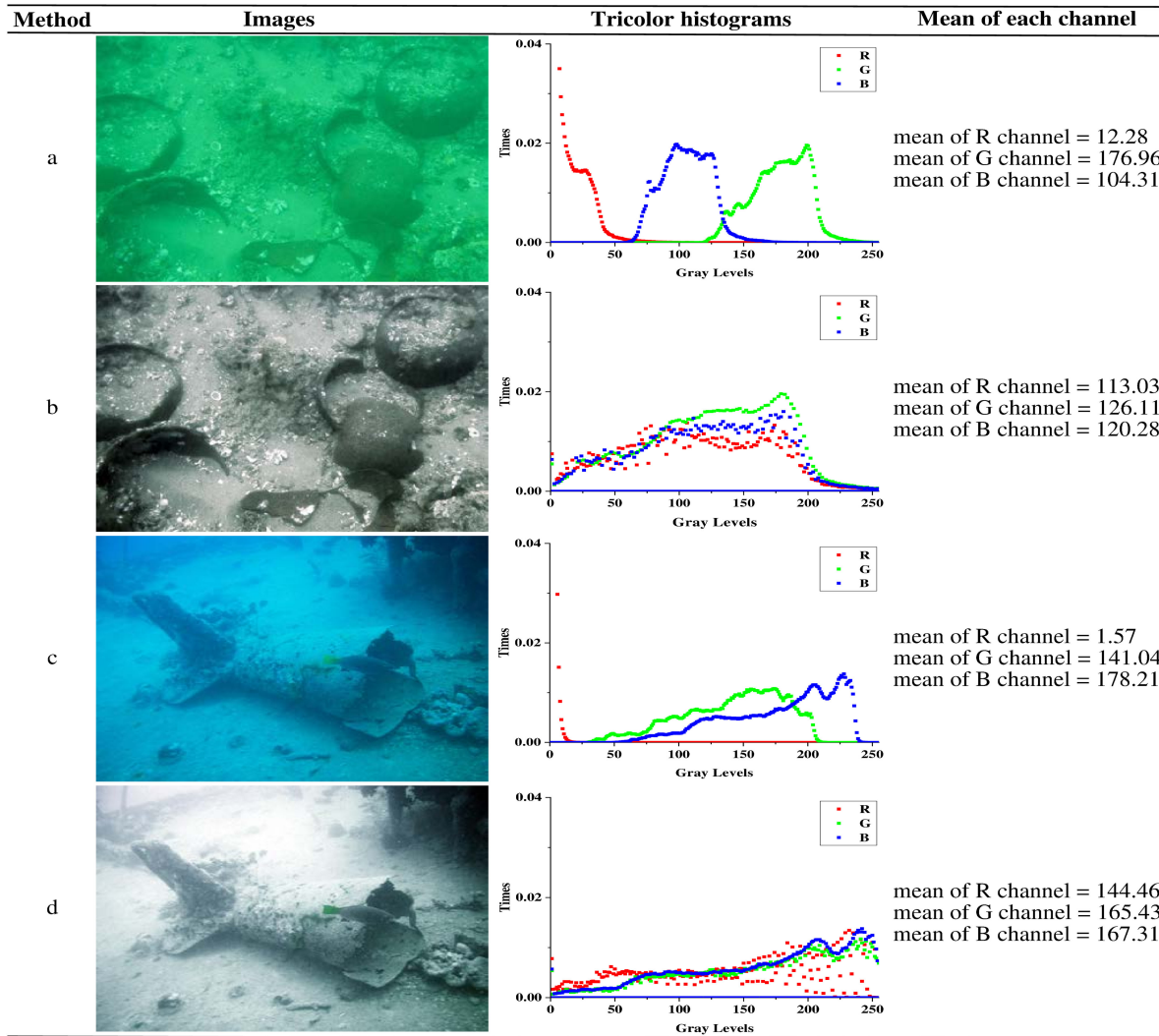


Fig. 3. Two types of degraded underwater image with our color-corrected results and the corresponding tricolor histograms. (a) and (c) Underwater images where the green and blue channels are well preserved, respectively. (b) and (d) Color-corrected results of our method applied to (a) and (c), respectively.

light source. Therefore, it is significant to divide the underwater image into background and foreground subimages. Based on this observation, the proposed method employs an iterative threshold strategy to determine the optimal separation point.

In the first step, the current underwater image is decomposed into red, green, and blue channels. Next, the minimum, maximum, and optimal separation points are determined for the three-color channels. More specifically, the minimum-intensity value is determined based on the lowest-intensity value of the image histogram. The maximum-intensity value is determined based on the highest intensity value of the image histogram. The optimal separation point is determined by the iterative threshold strategy. Additionally, the foreground (the histogram of high pixel values) and the background (the histogram of low pixel values) of each channel are separated, as detailed in Algorithm 1.

After the optimal separation point is determined, the histograms of the red, green, and blue channels are divided into two histograms, namely, background-stretched histograms and

foreground-stretched histograms. Then, the background histograms are stretched from the minimum-intensity value I_{\min} to the optimal separation threshold I_{opt} of the dynamic range, while the foreground histograms are stretched from the optimal separation threshold I_{opt} to the maximum-intensity value I_{\max} of the dynamic range. Thus, the background and foreground histograms are stretched as follows:

$$I_B = I_{\min} + (I_{\text{opt}} - I_{\min}) \times \text{CDF}(I_{\text{CR}}), \quad I_{\text{CR}} \in [I_{\min}, I_{\text{opt}}] \quad (7)$$

$$I_F = (I_{\text{opt}} + 1) + (I_{\max} - (I_{\text{opt}} + 1)) \times \text{CDF}(I_{\text{CR}}), \quad I_{\text{CR}} \in [I_{\text{opt}}, I_{\max}] \quad (8)$$

where I_B and I_F are the background-stretched and foreground-stretched histograms for each color channel, respectively. I_{CR} and $\text{CDF}()$ are the color-corrected image and the cumulative distribution function (CDF), respectively. I_{\min} and I_{\max} are the minimum and maximum values of the current image, respectively.

Algorithm 1: Separation of the Foreground and Background of Each Color Channel

```

1: Input:  $I_{CR}^c(x), c \in \{R, G, B\}$ .
2: for each  $c \in \{R, G, B\}$  do
3:   Initialize:  $Loss = 1, I_{\min} = \min(I_{CR}^c), I_{\max} = \max(I_{CR}^c), Num1 = 0, Num2 = 0, S1 = 0, S2 = 0, I_{\text{init}} = (I_{\min} + I_{\max})/2$ .
4:   while  $Loss \geq 0.5$  do
5:     for each  $i \in [1, M], j \in [1, N]$  do
6:       if  $I_{CR}^c(i, j) > I_{\text{init}}$  then
7:          $Num1 = Num1 + 1, S1 = S1 + I_{CR}^c(i, j);$ 
8:       else
9:          $Num2 = Num2 + 1, S2 = S2 + I_{CR}^c(i, j);$ 
10:      end if
11:    end for
12:     $Mean_{S1} = S1/Num1;$ 
13:     $Mean_{S2} = S2/Num2;$ 
14:     $I_{\text{new}} = (Mean_{S1} + Mean_{S2})/2;$ 
15:    Update the constraint  $Loss = |I_{\text{init}} - I_{\text{new}}|$ ;
16:     $I_{\text{init}} = I_{\text{new}};$ 
17:    if  $Loss \geq 0.5$  then
18:       $Num1 = 0, Num2 = 0, S1 = 0, S2 = 0;$ 
19:    end if
20:  end while
21:   $I_{\text{opt}} = I_{\text{init}};$ 
22:  for each  $i \in [1, M], j \in [1, N]$  do
23:    if  $I_{CR}^c(i, j) < I_{\text{opt}}$  then
24:       $I_B^c(i, j) = I_{CR}^c(i, j);$ 
25:    else
26:       $I_F^c(i, j) = I_{CR}^c(i, j);$ 
27:    end if
28:  end for
29: end for
30:  $I_B = \sum \{I_B^R, I_B^G, I_B^B\};$ 
31:  $I_F = \sum \{I_F^R, I_F^G, I_F^B\};$ 
32: Output:  $I_B$  and  $I_F$ ;
  
```

The background and foreground images are stretched within the corresponding dynamic range. For the red, green, and blue channels, the original histograms divided by the optimal threshold point will produce two histograms, namely, background-stretched histograms and foreground-stretched histograms. All background-stretched histograms are composed to generate an underenhanced image. Likewise, all foreground-stretched histograms are composed to generate an overenhanced image. Then, the under- and over-enhanced images are integrated into the enhanced image I_{BF} based on the optimal threshold point I_{opt} . Besides, Fig. 4 gives an illustration of the under- and over-enhanced images being integrated into the global contrast-improved image.

2) *Limited Histogram With Rayleigh Distribution:* Some methods [45], [46] have demonstrated that the Rayleigh distribution is ideal for maintaining the naturalness of underwater images. The distribution refers to the bell-shaped intensity-level distribution, which is concentrated in the intermediate intensity

level. The intensity levels in the image histogram of each channel are mapped according to the Rayleigh distribution. According to [45] and [46], the probability distribution function (PDF) and CDF of the Rayleigh distribution can be written as

$$\text{PDF}_R = \left(\frac{I_{CR}(i, j)}{\alpha^2} \right)^{e^{(-I_{CR}(i, j)^2/2\alpha^2)}} \quad (9)$$

$$\text{CDF}_R = 1 - e^{(-I_{CR}(i, j)^2/2\alpha^2)} \quad (10)$$

where $I_{CR}(i, j)$ refers to the pixel of the color-corrected image and α represents the distribution parameter of the Rayleigh distribution. The parameter α is set to 0.4 as default in [45]. The proposed method applies the Rayleigh distribution to the histogram of the color-corrected image. Therefore, (6) is integrated into (11) to obtain the stretched Rayleigh distribution as

$$I_{RW} = \frac{\left[(I_{CR} - I_{\min}) \left(\frac{O_{\max} - O_{\min}}{I_{\text{high}} - I_{\text{low}}} \right) \right]}{\alpha^2} - \left[\frac{O_{\min} + (I_{CR} - I_{\min}) \left(\frac{O_{\max} - O_{\min}}{I_{\text{high}} - I_{\text{low}}} \right)}{2\alpha^2} \right]^2 \cdot e^{-e^{(-I_{CR}(i, j)^2/2\alpha^2)}}. \quad (11)$$

The proposed method also uses the limits in these stretching processes, which applies the limits to the output image instead of applying to the input image. For each channel, the minimum stretching value of the output image is set to the minimum intensity value of the original histogram if it is greater than 3.5% of the minimum intensity value of three RGB channels. Otherwise, the minimum intensity value of the output image is set to 3.5% of the minimum intensity value of three RGB channels. Mathematically, it can be expressed as

$$O_{c,\min} = \begin{cases} I_{c,\min}, & I_{c,\min} > 3.5\% \text{ of } I_c \\ 3.5\% \text{ of } I_c, & \text{otherwise,} \end{cases} \quad c \in \{R, G, B\} \quad (12)$$

where I_c denotes the entire dynamic range of the image. Likewise, the maximum stretching value of the output image is determined as

$$O_{c,\max} = \begin{cases} I_{c,\max}, & I_{c,\max} < 96.5\% \text{ of } I_c \\ 96.5\% \text{ of } I_c, & \text{otherwise} \end{cases} \quad c \in \{R, G, B\} \quad (13)$$

where the limit levels of the minimum and maximum intensity values are set according to the methods in [45] and [46]. From the statistics, we found that 3.5% and 96.5% can make a good tradeoff between the local contrast and the global visual quality of the enhanced results. In addition, such hyperparameters avoid the underenhancement and overenhancement in the results.

Since the dynamic range is compressed after improving the global contrast, the local contrast is reduced (see the top-left image in Fig. 5). Consequently, the limited histogram with Rayleigh distribution is designed to improve the local contrast of the output image, which is directly applied to the color-corrected image. As the bottom-left image shown in Fig. 5, the limits and Rayleigh distribution are used to improve the local contrast and naturalness of the output image, respectively.

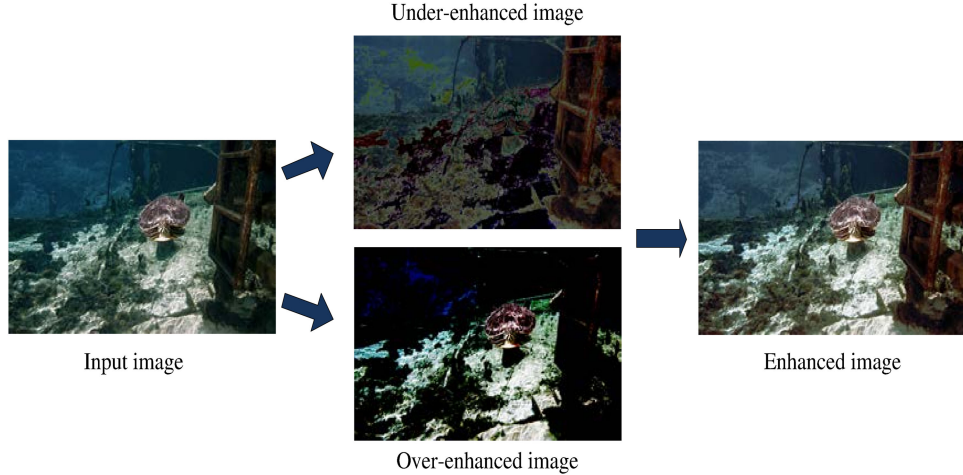


Fig. 4. Integration process of under- and over-enhanced images to produce the enhanced image. The integrated image can effectively avoid under- or over-enhancement.

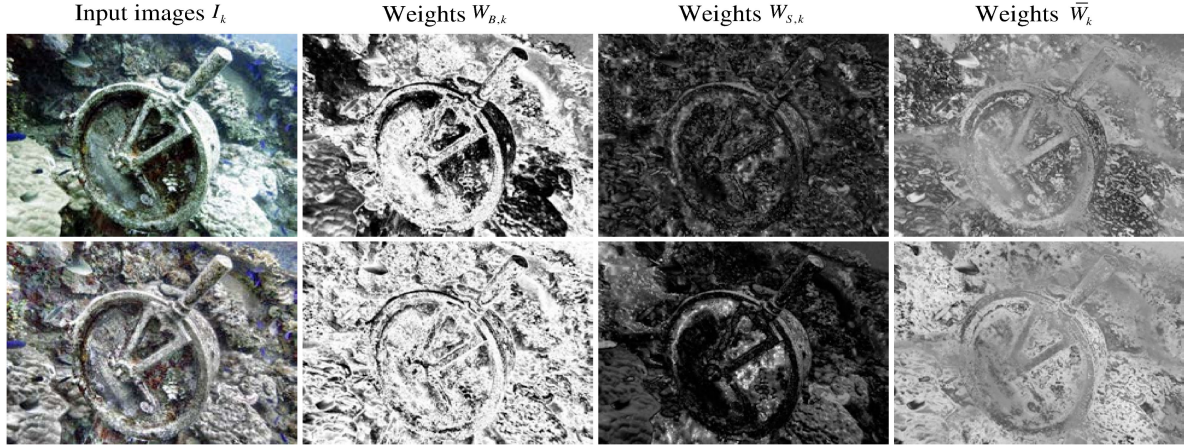


Fig. 5. Visual results of weight maps. Input images: top is the global contrast-improved version; bottom is the local contrast-improved version. Weights maps: brightness weights $W_{B,k}$, saliency weights $W_{S,k}$, and normalized weights \bar{W}_k .

C. Multiscale Fusion

The weight maps are used to make it easier for pixels with larger weight values to be displayed in the final result (see Fig. 2). We use two weight maps to fuse the global contrast-improved and the local contrast-improved versions. We detail the weight maps as follows.

Brightness weight map ($W_{B,k}$) is used to assign large values to well-exposed pixels. A high-quality image should be neither too bright nor too dark. Commonly, the pixels tend to have a higher exposed appearance when the mean value approximately equals 0.5 and the average of the standard deviations approximately equals 0.25 [68]. In the CIELAB color space, the brightness weight $W_{B,k}$ is expressed as a Gaussian-modeled distance to the mean normalized range value

$$W_{B,k}(i, j) = \exp \left(-\frac{(L_k(i, j) - 0.5)^2}{2 \times (0.25)^2} \right) \quad (14)$$

where $L_k(i, j)$ is the pixel value of the input image I_k at position (i, j) . $W_{B,k}$ is to highlight the contrast between light and dark areas (see the second column in Fig. 5).

Saliency weight map ($W_{S,k}$) is used to highlight saliency regions of the image and increase the contrast between the brightness and darkness regions. In addition, we consider the hue, saturation, and value of the input image. Therefore, we calculate the saliency weight ($W_{S,k}$) in the HSV color space, which is expressed as

$$W_{S,k}(i, j) = (H_k(i, j) - MH_k)^2 + (S_k(i, j) - MS_k)^2 + (V_k(i, j) - MV_k)^2 \quad (15)$$

where H_k , S_k , V_k , MH_k , MS_k , and MV_k are the hue, saturation, value, mean hue, mean saturation, and mean value of the k th input image, respectively. $W_{S,k}$ is to highlight regions with high contrast caused by hue, saturation, and value (see the third column in Fig. 5).

In our method, the two weight maps for each input are fused in a single map as follows. For each input I_k , an intergraded W_s is first obtained by calculating the sum of the two weight maps ($W_{B,k}$) and ($W_{S,k}$). Then, the normalized weight map \overline{W}_k is obtained for each input as

$$\overline{W}_k = (W_k + \beta) / \left(\sum_{k=1}^K W_k + K \cdot \beta \right),$$

where β is a small regularization term that ensures each input image contributing to the output image. We set β to 0.1 in our method. We show the examples of normalized weight maps in the fourth column of Fig. 5. We use the inputs and weights to obtain the fused result as

$$I_{\text{fusion}}(x, y) = \sum_{k=1}^K \overline{W}_k(i, j) I_k(i, j). \quad (16)$$

Since the sum of each \overline{W}_k is equal to 1, the intensity scale of the result is guaranteed to be the same as the inputs. First, for each input image, I_k is decomposed by Laplacian pyramid and defined as $L_l\{I_k(i, j)\}$. \overline{W}_k is decomposed by Gaussian pyramid and defined as $G_l\{\overline{W}_k(i, j)\}$. Next, the Laplacian pyramid $L_l\{I_k(i, j)\}$ and $G_l\{\overline{W}_k(i, j)\}$ are fused by

$$I_l(x, y) = \sum_{k=1}^N G_l\{\overline{W}_k(i, j)\} L_l\{I_k(i, j)\}$$

at each pixel, where $I_l(i, j)$ is the Laplacian pyramid of the fusion image. Finally, the enhanced image is obtained by summing the fused contribution of all levels

$$I_{\text{final}}(x, y) = \sum_l U_d[I_l(i, j)] \quad (17)$$

where $I_{\text{final}}(i, j)$ is the final output image and $U_d[I_l(i, j)]$ represents the upsampling operator with factor $d = 2^{l-1}$.

D. Multiscale Unsharp Masking

Unsharp masking is an effective solution to sharpen an image. Traditional sharpening technique first uses a Gaussian kernel to blur the initial image and then subtracts the blurred image from the initial image. Unlike the traditional technique, an MSUM is proposed in our image-dehazing work [50]. However, too many Gaussian kernels will increase the time complexity. Considering this issue, we reduce the complexity of this unsharp masking method by selecting three Gaussians kernels with different scales to blur the initial image. Specifically, the blurred formula is expressed as

$$I_{\text{Blur}}(i, j) = G_n(i, j) * I_{\text{Input}}(i, j) \quad (18)$$

where

$$G_n(x, y) = \frac{1}{2\pi\sigma_n^2} \exp\left(-\left(x^2 + y^2\right)/(2\sigma_n^2)\right)$$

represents a Gaussian kernel function, n is the number of filtering scales of the Gaussian kernel function, and $*$ is convolution operation. We refer to [50] to determine three scales within the interval of $0 < \sigma_1 \leq 50$, $50 < \sigma_2 \leq 100$, and $100 < \sigma_3$,

respectively. Concretely, for each color channel, the three blurred images are merged in a single blurred image as follows.

For each color channel, the three blurred images are first obtained by (18). Next, the three blurred images are integrated into one blurred image as

$$I_{\text{Blur}} = \sum_{n=1}^N I_{\text{Blur}}_n / N.$$

Subsequently, a sharpened image is obtained by subtracting the blurred image from the input image. In addition, a linear normalization operation is introduced so that the set of differential pixel values is uniformly distributed over the dynamic range. Finally, the sharpened image is obtained by

$$I_{\text{sharp}} = I_{\text{Input}} + T\{I_{\text{Input}} - I_{\text{Blur}}\} \times \eta \quad (19)$$

where $T\{\cdot\}$ is the linear normalization operation and η is a parameter that controls the strength of the desired sharpening result. In practice, a small η fails to sharpen I_{Input} , but a large η results in oversaturated regions. In our method, η is set to 1.5 empirically.

In Fig. 6, we show the step-by-step results of our framework. From Fig. 6, the following observation can be found: 1) the color-corrected image has natural color, but the low contrast and lost details are not improved; 2) the global contrast-improved image has high global contrast and sharp details, but the central area is too bright and the surrounding area is too dark; 3) the local contrast-improved image has high local contrast, but the surrounding area is too bright and local details are lost; 4) the fused image integrates the complementary advantages between the global and local contrast-improved images; and 5) the sharpened image further enhances the local details and edge textures.

IV. EXPERIMENTAL RESULTS

In this part, we conduct comprehensive evaluations among different methods. The proposed method is compared with 12 methods, namely, UDCP [25], MLHP [27], IBLA [28], RFEM [29], GDPC [30], CBAF [52], GLHDF [53], CCACE [54], CCBE [55], FUNIEGAN [42], DUIENet [43], and UIEC²-Net [44]. Among them, UDCP [25], MLHP [27], IBLA [28], RFEM [29], and GDPC [30] are restoration-based methods, while CBAF [52], GLHDF [53], CCACE [54], and CCBE [55] are enhancement-based methods. FUNIEGAN [42], DUIENet [43], and UIEC²-Net [44] are deep-learning-based methods. We use the recommended parameter settings to run the source codes provided by the authors to output the best results of different methods.

We conduct experiments on four underwater image enhancement benchmark data sets (UIEB [43], EUVP [42], UCCS [56], and OceanDark [57]). UIEB and EUVP aim to implement a comprehensive perceptual study and analysis for underwater image enhancement methods. UIEB contains 950 real-world underwater images collected from the Internet. EUVP contains over 12 K paired and 8 K unpaired underwater images. UCCS aims to evaluate the color correction capabilities of different methods for underwater images. It contains three 100-image subsets of the bluish, greenish, and blue-green tones collected



Fig. 6. (a)–(f) Step-by-step results in our framework. (a) Raw underwater image, (b) color-corrected image, (c) global contrast-improved image, (d) local contrast-improved image, (e) fused image, (f) sharpened image (top row), and their corresponding amplified details (bottom row), respectively.

by an undersea image capture system in the Zhangzi island of the Yellow Sea. OceanDark aims to evaluate the performance of different methods for enhancing the global and local contrast of underwater images. It contains 183 samples of low-light underwater images captured by Ocean Networks Canada.

A. Comprehensive Evaluation on UIEB

1) *Qualitative Evaluation:* UIEB contains a variety of degraded underwater images and is widely applied to evaluate underwater image enhancement methods. Therefore, we first select several typical underwater images from UIEB and then divide these images into five categories according to their appearance: greenish images, bluish images, yellowish images, hazy images, and low-light images. The results enhanced by different methods are shown in Fig. 7. Due to the limited space, we only show parts of the representative results of different methods.

In the open ocean, the red light first disappears due to its longest wavelength followed by the green light, the blue light, and the yellow light [10]. Such selective attenuation results in greenish, bluish, or yellowish underwater images, such as the raw underwater images in the first three rows of Fig. 7(a). For the greenish, bluish, and yellowish underwater images, MLHP [27], RFEM [29], and FUNIEGAN [42] introduce reddish color cast due to the inaccurate color correction methods applied to MLHP [27], RFEM [29], and FUNIEGAN [42]. CBAF [52] and DUIENet [43] remove the color cast well, while the performance of CBAF [52] and DUIENet [43] for contrast enhancement is unsatisfactory. UDCP [25] and IBLA [28] have a less positive effect on the enhancement of greenish, bluish, and yellowish underwater images, while GDPC [30] exacerbates the color distortion of greenish, bluish, and yellowish images. GLHDF [53] enhances the contrast well but produces darkness in local regions. Although CCACE [54] and CCBE [55] achieve satisfactory performance in contrast enhancement, they introduce overenhanced areas in the results. UIEC $\hat{2}$ -Net [44] improves the color and contrast of underwater images well, but it is inferior to our method in terms of detail sharpening. Additionally, our method achieves satisfactory results in terms of color correction, contrast enhancement, and detail sharpening.

For the underwater images with haze and low light, as shown in the last two rows of Fig. 7(a), MLHP [27], IBLA [28], GLHDF [53], CCACE [54], CCBE [55], and UIEC $\hat{2}$ -Net [44]

significantly remove the effects of haze on the underwater images, while UDCP [25], CBAF [52], and DUIENet [43] remain some haze in the results. RFEM [29] and FUNIEGAN [42] introduce reddish color deviations, while GDPC [30] aggravates the effects of haze. For the low-light case, MLHP [27], CCACE [54], CCBE [55], and UIEC $\hat{2}$ -Net [44] significantly remove the effects of darkness in the results, while UDCP [25], IBLA [28], CBAF [52], GLHDF [53], FUNIEGAN [42], and DUIENet [43] remain some dark regions in the enhanced results. We note that RFEM [29] and GDPC [30] tend to bring in color casts in the results. Besides, FUNIEGAN [42] and DUIENet [43] lost details in the results. UDCP [25] and GDPC [30] have a less positive effect on the underwater images with darkness and bluish tone. MLHP [27] and CCBE [55] produce overenhanced regions in the results. In contrast, our method effectively removes the effects of haze and low light and enhances the contrast and textures.

2) *Quantitative Evaluation:* To quantitatively evaluate the performance of our method, we compare it against 12 methods under five commonly used image quality evaluation metrics, including average gradient (AG) [50], information entropy (IE) [50], edge intensity (EI) [67], patch-based contrast quality index (PCQI) [69], and underwater image quality metric (UIQM) [70]. A higher AG [50] score suggests that the result has better visibility. A higher IE [50] score suggests that the result has more color information. A higher EI [67] score suggests that the result has better edges. A higher PCQI [69] score suggests that the result has better contrast. UIQM [70] uses underwater image colorfulness measure, underwater image sharpness measure, and underwater image contrast measure to evaluate the quality of underwater images. A higher UIQM [70] score suggests the result has better colorfulness, sharpness, and contrast.

Table I shows the average quantitative scores of different methods on UIEB. Our method achieves the best results across all quantitative evaluation metrics. These quantitative results demonstrate the effectiveness and robustness of our method.

B. Comprehensive Evaluation on EUVP

1) *Qualitative Evaluation:* We select several representative underwater images from the 515 test samples of the EUVP data set and grouped them into four categories: greenish images, low-visibility images, hazy images, and low-light images.

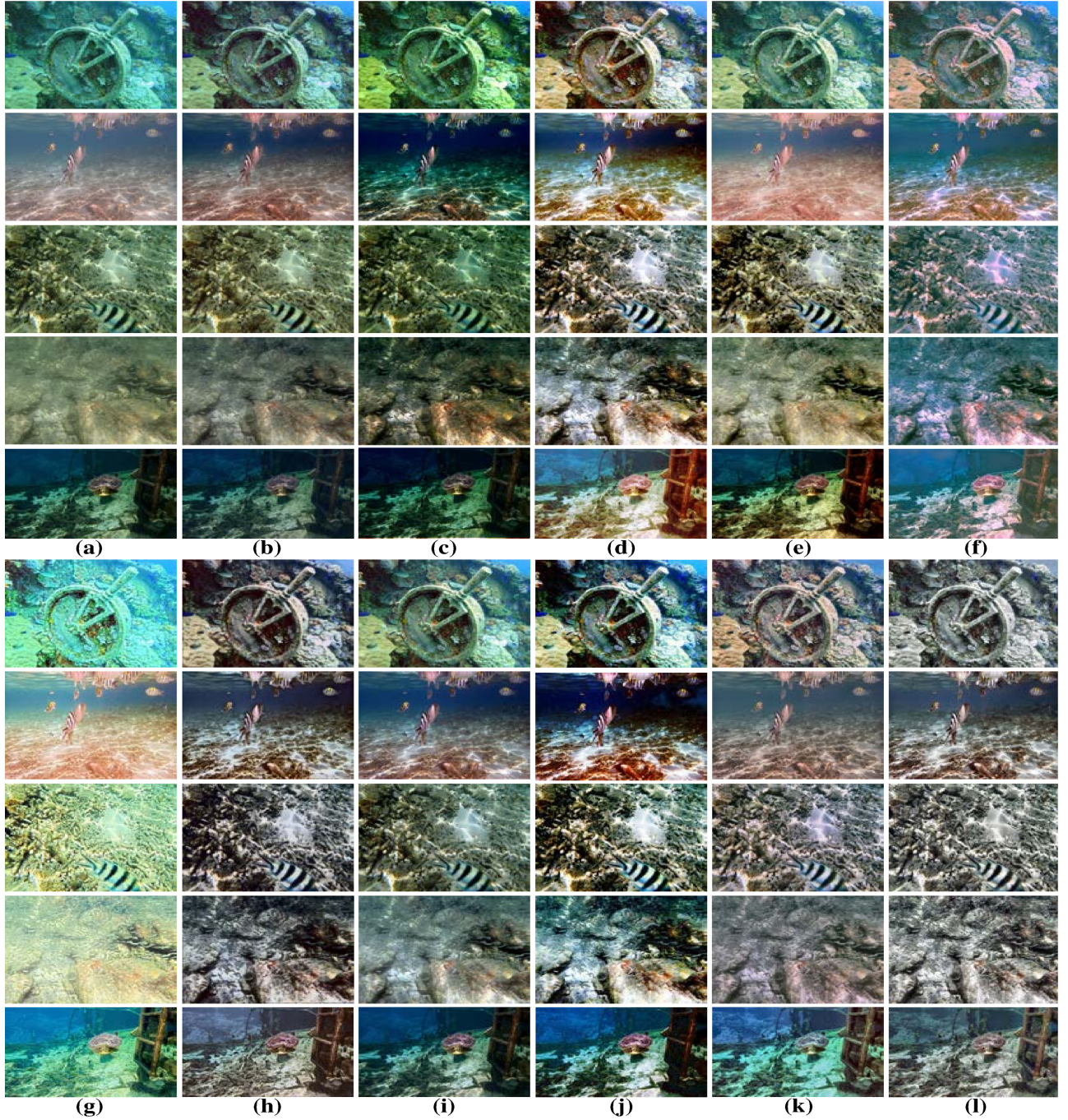


Fig. 7. Qualitative comparisons on UIEB. (a) Five raw underwater images sampled from UIEB. From top to bottom are the images with greenish color, bluish color, yellowish color, heavy haze, and limited lighting, respectively. The results enhanced using (b) UDCP [25], (c) MLHP [27], (d) IBLA [28], (e) RFEM [29], (f) GDCP [30], (g) CBAF [52], (h) GLHDF [53], (i) CCACE [54], (j) CCBE [55], (k) FUNIEGAN [42], (l) DUIENet [43], (m) UIEC²-Net [44], and (n) the proposed method.

Due to the limited space, we only show part of the experimental results of different methods in Fig. 8. UDCP [25], IBLA [28], GDCP [30], and FUNIEGAN [42] do not remove the green distortion well. Although MLHP [27], RFEM [29], and CCACE [54] remove the green distortion, they introduce the reddish distortion. CBAF [52] and GLHDF [53] demonstrate good performance in color correction, dehazing, and contrast enhancement, but they are not satisfactory for low-light image

enhancement. The enhanced results of DUIENet [43] introduce local darkness. CCBE [55] and UIEC²-Net [44] can obtain satisfactory results, but they are weaker than our method in terms of detail highlighting and visibility improvement.

2) *Quantitative Evaluation:* Table II reports the quantitative scores of different methods averaged in the EUVP data set. Our method obtains the highest AG [50], IE [50], EI [67], and PCQI [69] values, and the second best UIQM [70] value.

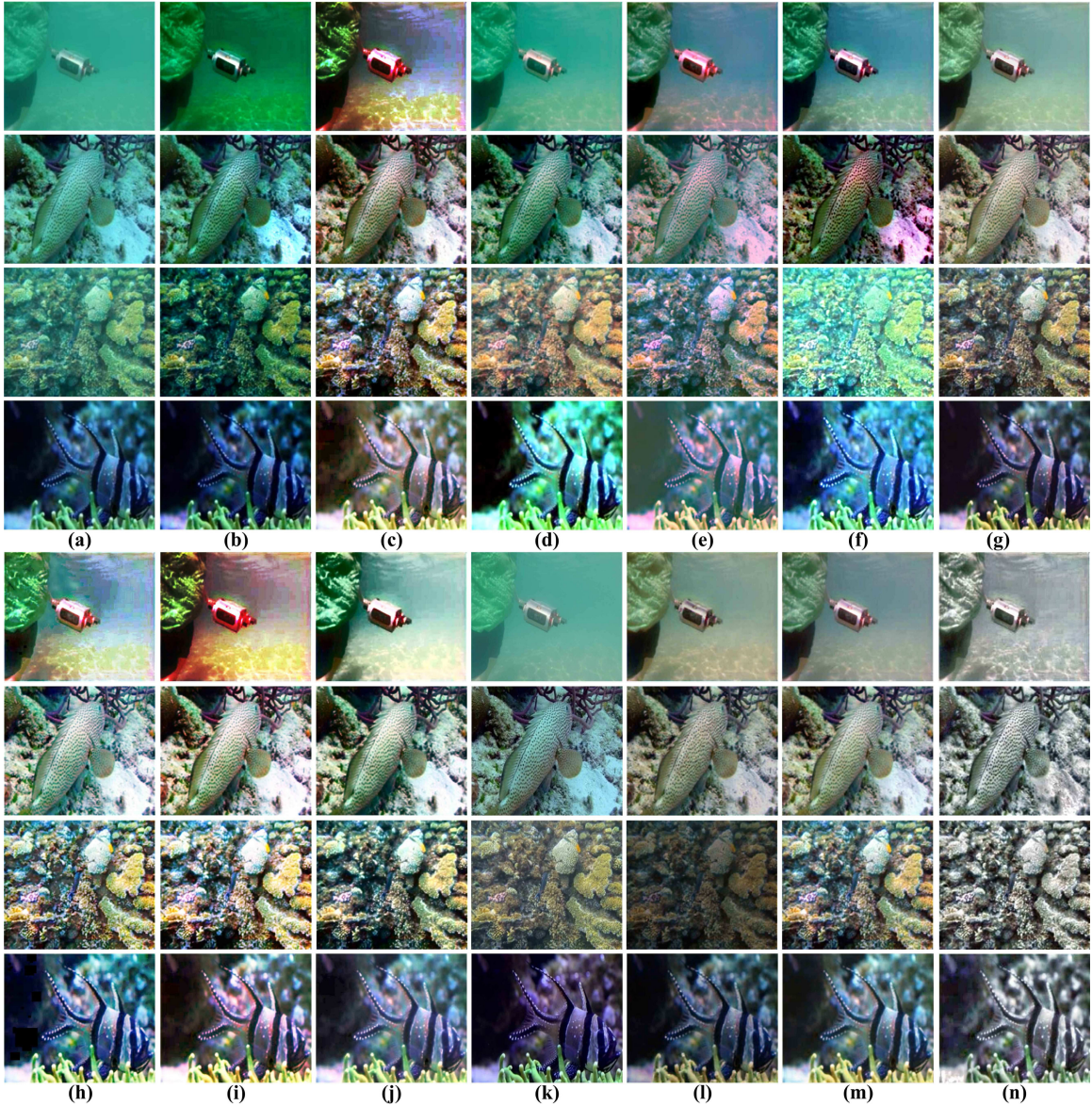


Fig. 8. Qualitative comparisons on EUVP. (a) Four raw underwater images sampled from EUVP. From top to bottom are the images with greenish color, low visibility, heavy haze, and limited lighting, respectively. The results enhanced using (b) UDCP [25], (c) MLHP [27], (d) IBLA [28], (e) RFEM [29], (f) GDCP [30], (g) CBAF [52], (h) GLHDF [53], (i) CCACE [54], (j) CCBE [55], (k) FUnIEGAN [42], (l) DUIENet [43], (m) UIEC $\hat{2}$ -Net [44], and (n) the proposed method.

Therefore, our method has relatively better enhanced performance than these compared methods for the testing data of EUVP data set.

C. Color Correction Evaluation on UCCS

Different wavelengths of light, water depth, salinity, and temperature of water cause serious color casts of underwater images. We compare our method with 12 methods on UCCS to evaluate the performance of different methods for color correction. The visual results of different methods are shown in Fig. 9.

1) Qualitative Evaluation: Due to the limited space, Fig. 9 only presents the representative results of different methods. Note that these images are three samples randomly selected from the three 100-image subsets with blue, green, and blue-green images, respectively. At this point, we focus on the

comparisons of color correction. MLHP [27], RFEM [29], GLHDF [53], CCACE [54], and CCBE [55] can correct both greenish and bluish tone well; however, they produce reddish results. IBLA [28] and GDCP [30] correct the blue-green underwater images well. However, they tend to fail in the bluish and greenish underwater images. The CBAF [52] handles blue images better than blue-green images. UDCP [25] and DUIENet [43] produce darkness for greenish underwater images. FUnIEGAN [42] introduces yellowish color deviations for green and blue-green images. UIEC $\hat{2}$ -Net [44] and our method can handle both bluish, greenish, and bluish-greenish tones well, but UIEC $\hat{2}$ -Net [44] is inferior to our method in terms of visibility.

2) Quantitative Evaluation: Table III reports the quantitative scores of different methods averaged in the three subdata sets of UCCS. For the Blue and Blue-green data sets, it can be observed that our method stands out among the compared methods except

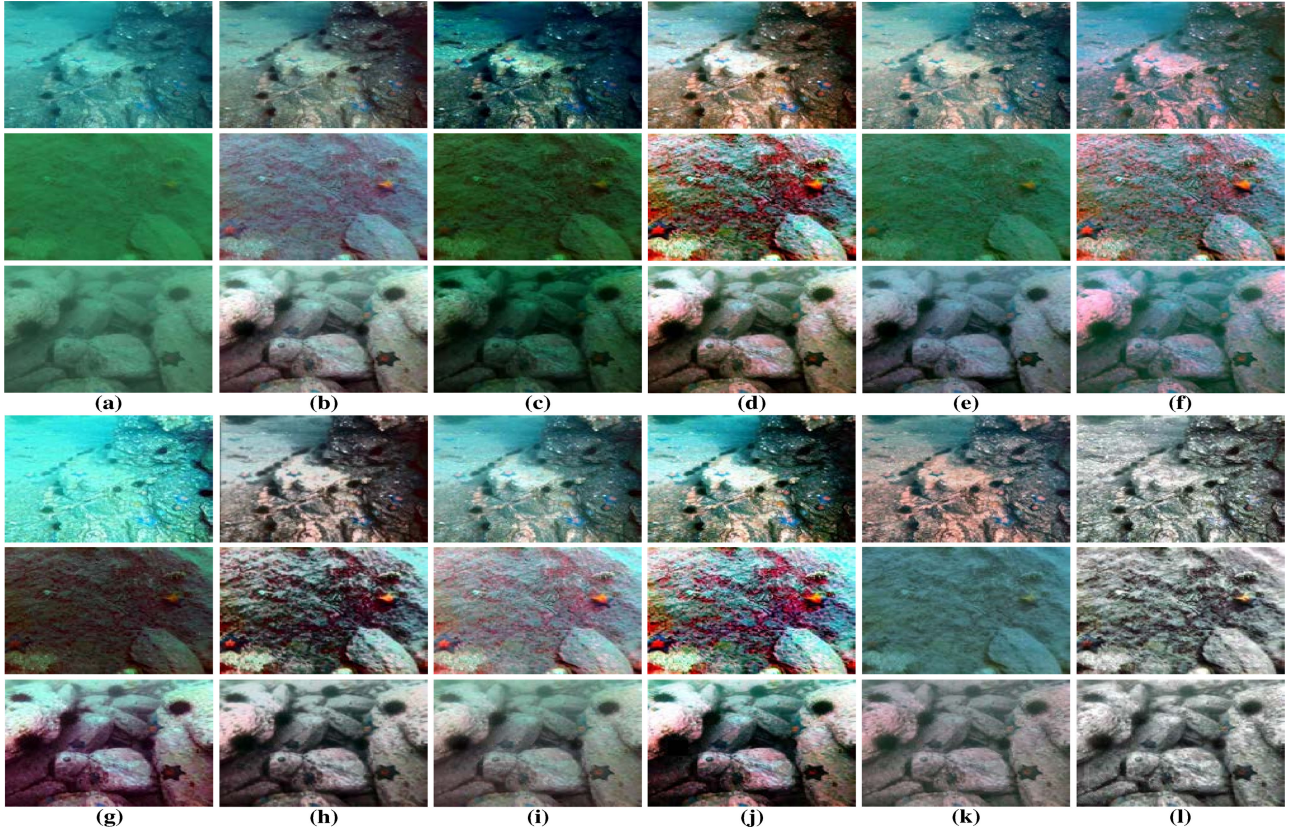


Fig. 9. Qualitative comparisons on UCCS. (a) Three raw underwater images sampled from UCCS. From top to bottom are the images selected from the subsets Blue, Green, and Blue-green of UCCS, respectively. The results enhanced using: (b) UDCP [25], (c) MLHP [27], (d) IBLA [28], (e) RFEM [29], (f) GDCP [30], (g) CBAF [52], (h) GLHDF [53], (i) CCACE [54], (j) CCBE [55], (k) FUNIEGAN [42], (l) DUEINet [43], (m) UIEC $\hat{2}$ -Net [44], and (n) the proposed method.

TABLE I

QUANTITATIVE SCORES IN TERMS OF THE AVERAGE VALUES OF AG, IE, EI, PCQI, AND UIQM OF DIFFERENT METHODS ON UIEB

Methods	AG \uparrow	IE \uparrow	EI \uparrow	PCQI \uparrow	UIQM \uparrow
UDCP [25]	5.673	6.781	56.014	0.905	3.358
MLHP [27]	8.319	7.337	82.080	1.091	4.016
IBLA [28]	6.035	7.247	59.577	1.071	2.825
RFEM [29]	6.491	7.508	64.089	1.031	3.365
GDCP [30]	7.208	7.275	70.888	1.042	3.264
CBAF [52]	6.581	7.543	64.222	1.044	3.642
GLHDF [53]	9.111	7.148	88.481	1.077	3.054
CCACE [54]	9.564	7.296	93.770	1.104	3.893
CCBE [55]	9.441	7.579	91.633	1.055	3.472
FUNIEGAN [42]	4.852	7.504	54.545	0.782	3.440
DUEINet [43]	4.428	7.005	53.054	0.851	3.798
UIEC $\hat{2}$ -Net [44]	6.692	7.689	66.295	1.061	4.079
Ours	9.968	7.703	98.693	1.146	4.347

The bold scores denote the best results under each case.

for the IE [50] scores, and the IE [50] scores are almost close to the highest values. For the Green data set, our method achieves the highest UIQM [70] score, but the AG [50], IE [50], EI [67],

TABLE II

QUANTITATIVE SCORES IN TERMS OF THE AVERAGE VALUES OF AG, IE, EI, PCQI, AND UIQM OF DIFFERENT METHODS ON EUVP

Methods	AG \uparrow	IE \uparrow	EI \uparrow	PCQI \uparrow	UIQM \uparrow
UDCP [25]	6.681	7.049	70.245	0.933	4.258
MLHP [27]	9.414	7.500	98.496	1.078	5.225
IBLA [28]	7.733	7.357	81.370	1.042	3.600
RFEM [29]	6.992	7.521	73.400	0.949	4.055
GDCP [30]	9.570	7.472	100.246	1.047	3.128
CBAF [52]	7.844	7.535	81.545	1.027	4.577
GLHDF [53]	9.419	7.753	97.758	1.091	3.982
CCACE [54]	10.081	7.398	105.418	1.086	4.889
CCBE [55]	9.135	7.634	95.458	1.038	4.275
FUNIEGAN [42]	7.603	7.415	74.762	0.805	4.442
DUEINet [43]	6.145	7.256	63.895	0.844	4.568
UIEC $\hat{2}$ -Net [44]	7.681	7.661	80.501	1.023	4.416
Ours	11.284	7.734	117.076	1.114	4.985

The bold scores denote the best results under each case.

and PCQI [69] scores obtained by our method are lower than the highest values. Although MLHP [27], CBAF [52], and GLHDF [53] obtain the higher AG [50], EI [67], and PCQI [69]

TABLE III
QUANTITATIVE SCORES IN TERMS OF THE AVERAGE VALUES OF AG, IE, EI, PCQI, AND UIQM OF DIFFERENT METHODS ON UCCS

Methods	Blue					Green					Blue-green				
	AG ↑	IE ↑	EI ↑	PCQI ↑	UIQM ↑	AG ↑	IE ↑	EI ↑	PCQI ↑	UIQM ↑	AG ↑	IE ↑	EI ↑	PCQI ↑	UIQM ↑
UDCP [25]	7.674	6.844	73.936	0.931	2.122	2.404	6.475	24.919	1.076	2.594	3.095	6.899	32.204	1.011	2.971
MLHP [27]	11.906	7.375	113.916	1.149	4.530	8.376	6.704	86.462	1.268	3.603	6.290	7.104	65.415	1.237	3.619
IBLA [28]	7.519	7.484	72.286	1.096	2.499	2.900	6.944	30.033	1.199	1.203	2.934	7.204	30.520	1.134	1.595
RFEM [29]	8.661	7.549	83.178	1.086	3.634	6.955	7.505	71.578	1.212	2.825	5.079	7.606	52.674	1.203	2.859
GDCP [30]	9.679	7.442	92.879	1.096	1.863	3.342	6.861	34.497	1.128	2.429	3.791	7.169	39.270	1.089	3.445
CBAF [52]	8.917	7.622	81.911	1.117	4.100	7.128	7.803	74.571	1.205	4.126	5.964	7.813	62.782	1.170	3.965
GLHDF [53]	12.899	6.961	121.569	1.190	3.212	9.408	6.601	95.877	1.212	3.304	7.308	6.809	74.432	1.182	2.736
CCACE [54]	11.676	7.395	111.774	1.145	4.320	8.900	6.906	91.555	1.220	3.383	6.621	7.201	68.720	1.228	3.106
CCBE [55]	10.407	7.648	102.736	1.078	2.971	7.801	7.793	80.761	1.171	3.942	6.487	7.762	67.639	1.174	3.140
FUnIEGAN [42]	6.049	7.333	59.967	0.856	3.916	2.598	7.474	24.598	1.003	3.922	2.585	7.451	32.477	1.082	2.761
DUIENet [43]	6.424	7.183	61.914	0.901	3.894	4.205	7.392	43.778	1.069	3.571	3.903	7.408	40.521	1.055	3.163
UIEC ² -Net [44]	8.398	7.674	80.703	1.108	3.894	4.360	7.526	44.708	1.106	3.375	4.364	7.557	45.001	1.154	3.097
Ours	14.889	7.712	140.448	1.259	5.033	7.058	7.663	71.847	1.197	4.183	7.231	7.647	74.919	1.251	4.136

The bold scores denote the best results under each case.

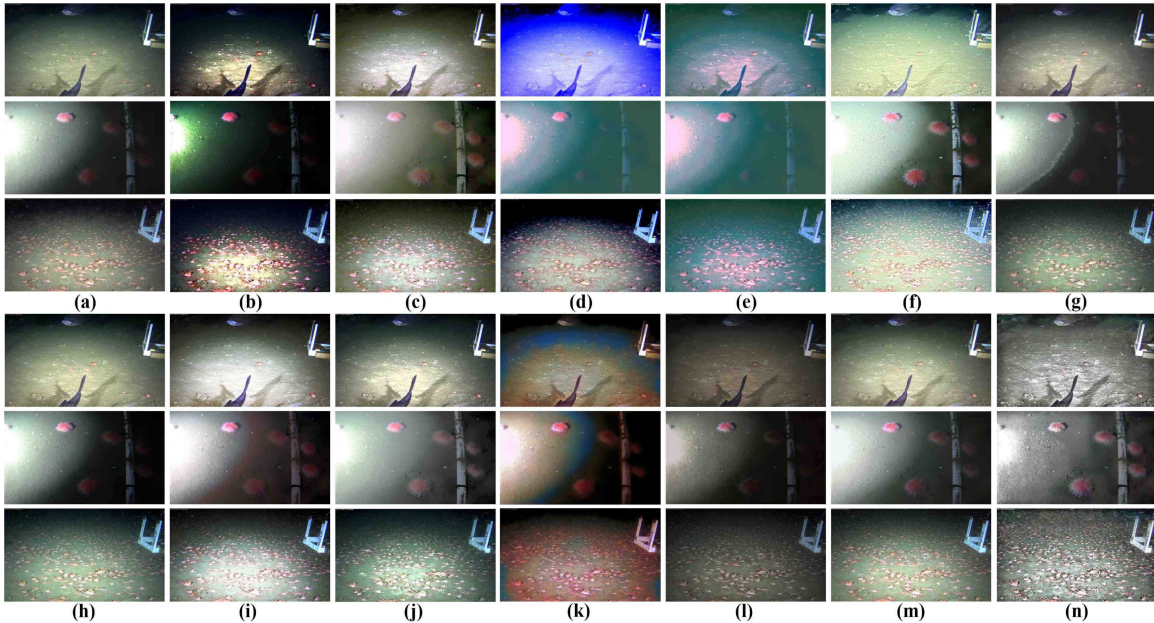


Fig. 10. Qualitative comparisons on OceanDark. (a) Three low-light underwater images sampled from OceanDark. From top to bottom are the results obtained using (b) UDCP [25], (c) MLHP [27], (d) IBLA [28], (e) RFEM [29], (f) GDCP [30], (g) CBAF [52], (h) GLHDF [53], (i) CCACE [54], (j) CCBE [55], (k) FUnIEGAN [42], (l) DUIENet [43], (m) UIEC²-Net [44], and (n) the proposed method.

scores, it can be found that it generates overcorrected reddish results for the Green data set from the subjective perspective perception. Therefore, the ability of our method for color correction of the Green data set is also satisfactory compared to other methods.

D. Contrast Enhancement Evaluation on OceanDark

In open deep water, insufficient light or limited artificial light seriously affects the quality of underwater images. These images commonly suffer from contrast degradations and darker appearance, such as the raw underwater images in Fig. 10(a). Achieving higher contrast and higher visibility is an important objective for underwater image enhancement methods. Therefore, we

compare our method with 12 methods on OceanDark to evaluate the performance of different methods for contrast enhancement.

1) *Qualitative Evaluation:* As shown in Fig. 10, UDCP [25], IBLA [28], RFEM [29], GDCP [30], and FUnIEGAN [42] aggravate the effects of color casts and contrast degradation. CBAF [52] and DUIENet [43] have a less positive effect on these images for contrast enhancement. MLHP [27], GLHDF [53], CCACE [54], and CCBE [55] still suffer from overenhancement in the central area of their results. Although UIEC²-Net [44] can significantly improve the contrast of some underwater images, our method outperforms it for the darker areas.

2) *Quantitative Evaluation:* The average quantitative scores are given in Table IV. Our method obtains the higher scores of AG [50], EI [67], PCQI [69], and UIQM [70] than the compared

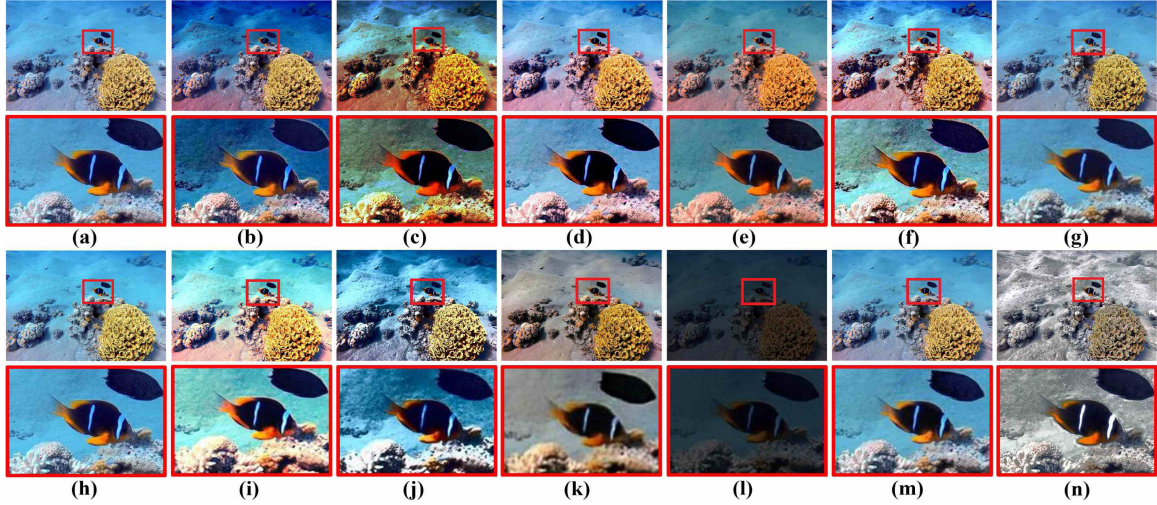


Fig. 11. Visual results of detail preserving for a representative underwater image selected from UIEB. (a) Raw underwater image. The results enhanced using (b) UDCP [25], (c) MLHP [27], (d) IBLA [28], (e) RFEM [29], (f) GDCP [30], (g) CBAF [52], (h) GLHDF [53], (i) CCACE [54], (j) CCBE [55], (k) FUNIEGAN [42], (l) DUIENet [43], (m) UIEC $\hat{2}$ -Net [44], and (n) the proposed method.

TABLE IV
QUANTITATIVE SCORES IN TERMS OF THE AVERAGE VALUES OF AG, IE, EI,
PCQI, AND UIQM OF DIFFERENT METHODS ON OCEANDARK

Methods	AG \uparrow	IE \uparrow	EI \uparrow	PCQI \uparrow	UIQM \uparrow
UDCP [25]	2.756	6.465	27.806	0.857	2.437
MLHP [27]	3.296	7.592	32.851	1.018	2.437
IBLA [28]	2.988	6.750	30.341	0.916	1.992
RFEM [29]	2.564	7.370	25.783	0.922	1.204
GDCP [30]	3.270	7.430	33.004	0.926	1.526
CBAF [52]	2.663	7.328	26.667	0.992	2.168
GLHDF [53]	3.871	7.206	38.272	0.994	2.563
CCACE [54]	3.356	7.570	33.533	1.018	2.439
CCBE [55]	2.823	7.436	31.778	1.026	2.828
FUNIEGAN [42]	2.473	7.194	25.810	0.865	2.575
DUIENet [43]	2.041	6.826	20.015	0.772	2.539
UIEC $\hat{2}$ -Net [44]	2.860	7.665	28.526	0.981	2.301
Ours	5.912	7.533	57.048	1.143	3.527

The bold scores denote the best results under each case.

methods and the similar IE [50] values with the best performer. Regarding the PCQI [69] score, our method is at least 10.2% better than the second-best performer. Therefore, the results indicate that our method has excellent contrast enhancement performance in both qualitative and quantitative metrics.

E. Detail-Preserving Analysis

For underwater image enhancement, fine details are also important for many practical applications [71]–[73], such as object detection and object tracking underwater. Nevertheless, the results produced by the existing methods tend to be excessively smooth, and the details are easily lost. In this section,

we compare the detail preserving of different methods. In addition, we only select a representative image from UIEB for comparisons due to the limited space. The enhanced results and enlarged regions from a representative test sample are shown in Fig. 11. As shown in the zoomed-in regions of each red box, the image enhanced by our method has a natural appearance, high visibility, and highlighted details.

F. Runtime

Runtime is an essential quantitative evaluation metric for a method to be applied in practical applications. Table V shows the average time of executing ten times of different methods on images of different resolutions. All methods are tested on a Windows 10 PC with Intel(R) Core(TM) i9-9900k CPU at 3.6 GHz, 48-GB memory, and NVIDIA GeForce GTX 1080Ti. Note that, limited by the network structure, FUNIEGAN [42] can only process images with a size of 256×256 . Deep-learning-based methods FUNIEGAN [42], DUIENet [43], and UIEC $\hat{2}$ -Net [44] have obvious advantages based on GPU acceleration. Our method is significantly faster than conventional methods UDCP [25], IBLA [28], RFEM [29], GLHDF [53], CCACE [54], and CCBE [55]. Although our method is slower than MLHP [27], GDCP [30], and CBAF [52], it outperforms them in terms of the enhancement quality of underwater images, as demonstrated in the aforementioned experiments.

G. Ablation Study

To demonstrate the effectiveness of each component in our method, we conduct the following ablation study on UIEB, UCCS, and OceanDark data sets, including: 1) our method without attenuated color channel correction (-w/o ACCC); 2) our method without dual-histogram-based iterative threshold selection (-w/o DHIT); 3) our method without limited histogram with Rayleigh distribution (-w/o LHRD); 4) our method without multiscale fusion (-w/o MSF); and 5) our method without

TABLE V
AVERAGE RUNTIME OF EACH METHOD FOR DIFFERENT IMAGE RESOLUTIONS (IN SECONDS)

Image Resolution	UDCP	MLHP	IBLA	RFEM	GDCP	CBAF	GLHDF	CCACE	CCBE	FUnIEGAN	DUIENet	UIEC^2-Net	Ours
256×256	4.37	0.33	8.68	55.98	0.61	0.23	0.91	0.82	0.88	0.12	1.04	0.24	0.85
512×512	18.90	1.15	34.57	126.71	2.57	0.64	3.65	2.87	2.93	-	1.23	1.08	2.86
768×768	44.64	2.71	83.99	254.41	6.08	1.79	8.62	6.88	6.92	-	2.23	2.51	6.44
1024×1024	77.02	4.34	143.75	383.31	8.16	3.00	14.10	11.05	10.97	-	3.48	4.43	10.78

"—" indicates the result is not available.

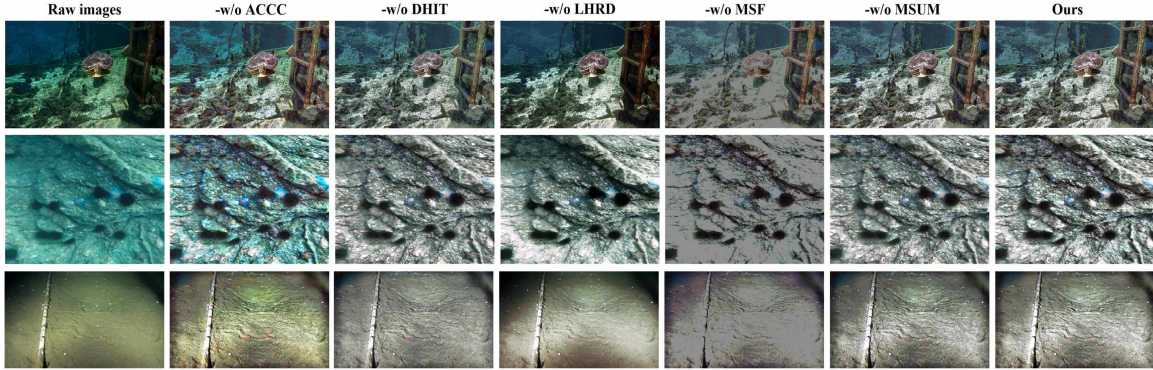


Fig. 12. Ablated results of our method. From top to bottom are three raw underwater images sampled from UIEB, UCCS, and OceanDark, respectively.

TABLE VI
ABLATION STUDY ON THE UIEB, UCCS, AND OCEANDARK DATA SETS

Methods	UIEB					UCCS					OceanDark				
	AG	IE ↑	EI ↑	PCQI ↑	UIQM ↑	AG ↑	IE ↑	EI ↑	PCQI ↑	UIQM ↑	AG ↑	IE ↑	EI ↑	PCQI ↑	UIQM ↑
-w/o ACCC	9.259	7.540	89.861	1.259	3.568	8.614	7.370	83.816	1.353	2.984	6.128	7.486	59.146	1.212	3.455
-w/o DHIT	9.023	7.556	87.742	1.126	4.265	8.885	7.517	87.452	1.220	4.329	5.478	7.421	53.025	1.146	3.433
-w/o LHRD	7.133	7.634	69.762	1.016	3.596	6.358	7.556	63.120	1.092	3.293	3.222	7.661	31.467	0.980	2.348
-w/o MSF	5.473	4.747	52.447	0.775	3.062	4.595	4.190	44.697	0.785	2.535	2.89	5.187	27.823	0.785	2.241
-w/o MSUM	9.196	7.670	90.574	1.135	4.283	9.177	7.666	91.518	1.233	4.415	4.898	7.506	48.894	1.152	3.307
Ours	9.968	7.703	98.693	1.146	4.347	9.726	7.674	95.738	1.236	4.450	5.912	7.533	57.048	1.143	3.527

The bold scores denote the best results under each case.

multiscale unsharp masking (-w/o USUM). The qualitative evaluations are performed on three representative underwater images sampled from UIEB, UCCS, and OceanDark, respectively. The quantitative evaluations are performed on the UIEB, UCCS, and OceanDark. The qualitative results of each component are presented in Fig. 12. The average scores in terms of AG [50], IE [50], EI [67], PCQI [69], and UIQM [70] are given in Table VI.

In Fig. 12, we can observe that more details can be obtained in the results produced by -w/o ACCC, but the color casts cannot be removed. The use of ACCC component has superior performance for color correction. The -w/o DHIT makes global contrast reduced, which suggests that the use of dual-histogram-based iterative threshold (DHIT) component improves the global contrast of the results. The -w/o LHRD reduces the local contrast and naturalness. The MSF component is used to fuse the lightness, hue, and saturation of the input images; however, the details of the fused image need to be improved further. The use of MSUM improves the structure and texture of the results.

The quantitative results of each component applied to UIEB, UCCS, and OceanDark data sets are provided in Table VI. Compared with the ablated models, the proposed method achieves similar and even higher values in terms of AG [50], IE [50], EI [67], PCQI [69], and UIQM [70] metrics. Although our method without the ACCC component obtains the highest PCQI [69] value, its performance for color correction is unsatisfactory, as shown in Fig 12. Therefore, these results demonstrate that all components used in our method have positive effects on the enhanced results.

H. Generalization Capability Evaluation of the Proposed Method

Although the main purpose of our method is to enhance underwater images, we found that our method also generalizes well to low-light images and hazy images [74], [75]. As shown in Fig. 13, it can be seen that the low-light images enhanced by our method look more natural and brighter, and the dehazed

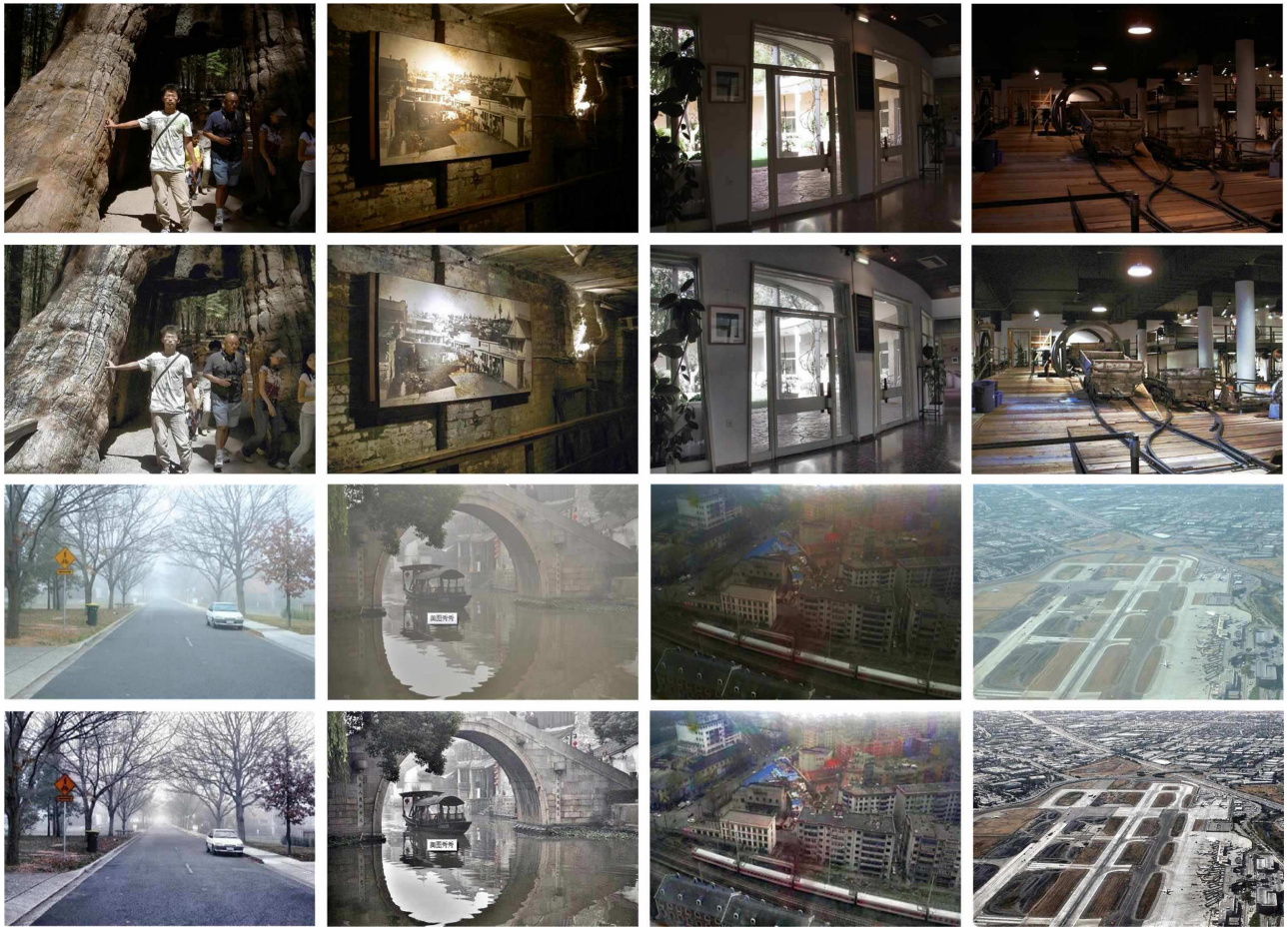


Fig. 13. Visual results of our method on low-light and hazy images. From top to bottom are the low-light images, the enhanced results by our method, the hazy images, and the results dehazed by our method.

images generated by our method remove the effects of haze. Note that these visually pleasing results are generated by our method without parameter fine-tuning, which indicates the good generalization capability of our method.

V. CONCLUSION

In this article, we proposed an underwater image enhancement method via ACCC and detail preserved contrast enhancement. The proposed method consists of a color correction method, a fusion-based contrast improvement method, and an MSUM method. Experiments on four underwater image enhancement benchmark data sets demonstrate that our method outperforms 12 underwater image enhancement methods in both qualitative and quantitative metrics. In addition, our method also generalizes well to low-light images and hazy images. In spite of the good performance, our method has some limitations. For example, the color of quality-degraded underwater images is reduced after enhancement by our method. In addition, the introduction of DHIT may increase computational complexity. In future work, we will focus on solving the aforementioned limitations.

REFERENCES

- [1] L. Chen *et al.*, "Perceptual underwater image enhancement with deep learning and physical priors," *IEEE Trans. Circuits Syst. Video Technol.*, vol. 31, no. 8, pp. 3078–3092, Aug. 2020.
- [2] P. Zhuang, C. Li, and J. Wu, "Bayesian Retinex underwater image enhancement," *Eng. Appl. Artif. Intell.*, vol. 101, 2021, Art. no. 104171.
- [3] H. Lu, T. Uemura, D. Wang, J. Zhu, Z. Huang, and H. Kim, "Deep-sea organisms tracking using dehazing and deep learning," *Mobile Netw. Appl.*, vol. 25, pp. 1008–1015, 2020.
- [4] W. Zhang, L. Dong, X. Pan, P. Zou, L. Qin, and W. Xu, "A survey of restoration and enhancement for underwater images," *IEEE Access*, vol. 7, pp. 182259–182279, 2019.
- [5] M. J. Islam, M. Fulton, and J. Sattar, "Toward a generic diver-following algorithm: Balancing robustness and efficiency in deep visual detection," *IEEE Robot. Autom. Lett.*, vol. 4, no. 1, pp. 113–120, Jan. 2019.
- [6] C. Li, J. Guo, and C. Guo, "Emerging from water: Underwater image color correction based on weakly supervised color transfer," *IEEE Signal Process. Lett.*, vol. 25, no. 3, pp. 323–327, Mar. 2018.
- [7] J. Yuan, W. Cao, Z. Cai, and B. Su, "An underwater image vision enhancement algorithm based on contour bougie morphology," *IEEE Trans. Geosci. Remote Sens.*, vol. 59, no. 10, pp. 8117–8128, Oct. 2021.
- [8] H. Lu *et al.*, "Underwater image enhancement method using weighted guided trigonometric filtering and artificial light correction," *J. Vis. Communun. Image Represent.*, vol. 38, pp. 504–516, 2016.
- [9] Y. Wang *et al.*, "An imaging-inspired no-reference underwater color image quality assessment metric," *Comput. Elect. Eng.*, vol. 70, pp. 904–913, 2018.

- [10] D. Akkaynak, T. Treibitz, T. Shlesinger, Y. Loya, R. Tamir, and D. Iluz, "What is the space of attenuation coefficients in underwater computer vision?", in *Proc. IEEE Conf. Comput. Vis. Pattern Recognit.*, 2017, pp. 568–577.
- [11] H. H. Chang, C. Y. Cheng, and C. C. Sung, "Single underwater image restoration based on depth estimation and transmission compensation," *IEEE J. Ocean. Eng.*, vol. 44, no. 4, pp. 1130–1149, Oct. 2019.
- [12] S. Anwar and C. Li, "Diving deeper into underwater image enhancement: A survey," *Signal Process.: Image Commun.*, vol. 89, 2020, Art. no. 115978.
- [13] S. G. Narasimhan and S. K. Nayar, "Contrast restoration of weather degraded images," *IEEE Trans. Pattern Anal. Mach. Intell.*, vol. 25, no. 6, pp. 713–724, Jun. 2003.
- [14] Y. Y. Schechner and Y. Averbuch, "Regularized image recovery in scattering media," *IEEE Trans. Pattern Anal. Mach. Intell.*, vol. 29, no. 9, pp. 1655–1660, Sep. 2007.
- [15] T. Treibitz and Y. Y. Schechner, "Turbid scene enhancement using multi-directional illumination fusion," *IEEE Trans. Image Process.*, vol. 21, no. 11, pp. 4662–4667, Nov. 2012.
- [16] T. Treibitz and Y. Y. Schechner, "Active polarization descattering," *IEEE Trans. Pattern Anal. Mach. Intell.*, vol. 31, no. 3, pp. 385–399, Mar. 2009.
- [17] H. Lu *et al.*, "Underwater image descattering and quality assessment," in *Proc. IEEE Int. Conf. Image Process.* 2016, pp. 1998–2002.
- [18] J. Li and Y. Li, "Underwater image restoration algorithm for free-ascending deep-sea trips," *Opt. Laser Technol.*, vol. 110, pp. 129–134, 2019.
- [19] C. Tan, G. Seet, A. Sluzek, and D. He, "A novel application of range-gated underwater laser imaging system (ULIS) in near-target turbid medium," *Opt. Lasers Eng.*, vol. 43, no. 9, pp. 995–1009, 2005.
- [20] K. Nomura, D. Sugimura, and T. Hamamoto, "Underwater image color correction using exposure-bracketing imaging," *IEEE Signal Process. Lett.*, vol. 25, no. 6, pp. 893–897, Jun. 2018.
- [21] J. S. Jaffe, "Computer modeling and the design of optimal underwater imaging systems," *IEEE J. Ocean. Eng.*, vol. 15, no. 2, pp. 101–111, Apr. 1990.
- [22] D. Akkaynak and T. Treibitz, "A revised underwater image formation model," in *Proc. IEEE/CVF Conf. Comput. Vis. Pattern Recognit.*, 2018, pp. 6723–6732.
- [23] K. He, J. Sun, and X. Tang, "Single image haze removal using dark channel prior," *IEEE Trans. Pattern Anal. Mach. Intell.*, vol. 33, no. 12, pp. 2341–2353, Dec. 2011.
- [24] J. Y. Chiang and Y. Chen, "Underwater image enhancement by wavelength compensation and dehazing," *IEEE Trans. Image Process.*, vol. 21, no. 4, pp. 1756–1769, Apr. 2012.
- [25] P. L. J. Drews, E. R. Nascimento, S. S. C. Botelho, and M. F. M. Campos, "Underwater depth estimation and image restoration based on single images," *IEEE Comput. Graph. Appl.*, vol. 36, no. 2, pp. 24–35, Mar./Apr. 2016.
- [26] C. Li, J. Guo, S. Chen, Y. Tang, Y. Pang, and J. Wang, "Underwater image restoration based on minimum information loss principle and optical properties of underwater imaging," in *Proc. IEEE Int. Conf. Image Process.*, 2016, pp. 1993–1997.
- [27] C. Li, J. Guo, R. Cong, Y. Pang, and B. Wang, "Underwater image enhancement by dehazing with minimum information loss and histogram distribution prior," *IEEE Trans. Image Process.*, vol. 25, no. 12, pp. 5664–5677, Dec. 2016.
- [28] Y. Peng and P. C. Cosman, "Underwater image restoration based on image blurriness and light absorption," *IEEE Trans. Image Process.*, vol. 26, no. 4, pp. 1579–1594, Apr. 2017.
- [29] C. Li, J. Guo, C. Guo, R. Cong, and J. Gong, "A hybrid method for underwater image correction," *Pattern Recognit. Lett.*, vol. 94, pp. 62–67, 2017.
- [30] Y. Peng, K. Cao, and P. C. Cosman, "Generalization of the dark channel prior for single image restoration," *IEEE Trans. Image Process.*, vol. 27, no. 6, pp. 2856–2868, Jun. 2018.
- [31] C. Dai, M. Lin, X. Wu, Z. Wang, and Z. Guan, "Single underwater image restoration by decomposing curves of attenuating color," *Opt. Laser Technol.*, vol. 123, 2020, Art. no. 105947.
- [32] M. Yang, A. Sowmya, Z. Wei, and B. Zheng, "Offshore underwater image restoration using reflection-decomposition-based transmission map estimation," *IEEE J. Ocean. Eng.*, vol. 45, no. 2, pp. 521–533, Apr. 2020.
- [33] Y. Zhou, Q. Wu, K. Yan, L. Feng, and W. Xiang, "Underwater image restoration using color-line model," *IEEE Trans. Circuits Syst. Video Technol.*, vol. 29, no. 3, pp. 907–911, Mar. 2019.
- [34] D. Berman, D. Levy, S. Avidan, and T. Treibitz, "Underwater single image color restoration using haze-lines and a new quantitative dataset," *IEEE Trans. Pattern Anal. Mach. Intell.*, vol. 43, no. 8, pp. 2822–2837, Aug. 2021.
- [35] J. Li, K. A. Skinner, R. M. Eustice, and M. Johnson-Roberson, "WaterGAN: Unsupervised generative network to enable real-time color correction of monocular underwater images," *IEEE Robot. Autom. Lett.*, vol. 3, no. 1, pp. 387–394, Jan. 2018.
- [36] X. Chen, J. Yu, S. Kong, Z. Wu, X. Fang, and L. Wen, "Towards real-time advancement of underwater visual quality with GAN," *IEEE Trans. Ind. Electron.*, vol. 66, no. 12, pp. 9350–9359, Dec. 2019.
- [37] Y. Guo, H. Li, and P. Zhuang, "Underwater image enhancement using a multiscale dense generative adversarial network," *IEEE J. Ocean. Eng.*, vol. 45, no. 3, pp. 862–870, Jul. 2020.
- [38] H. Lu, Y. Li, T. Uemura, H. Kim, and S. Serikawa, "Low illumination underwater light field images reconstruction using deep convolutional neural networks," *Future Gener. Comput. Syst.*, vol. 82, pp. 142–148, 2018.
- [39] C. Li, S. Anwar, and F. Porikli, "Underwater scene prior inspired deep underwater image and video enhancement," *Pattern Recognit.*, vol. 98, 2020, Art. no. 107038.
- [40] M. Yang, K. Hu, Y. Du, Z. Wei, Z. Sheng, and J. Hu, "Underwater image enhancement based on conditional generative adversarial network," *Signal Process.: Image Commun.*, vol. 81, 2020, Art. no. 115723.
- [41] X. Fu and X. Cao, "Underwater image enhancement with global-local networks and compressed-histogram equalization," *Signal Process.: Image Commun.*, vol. 86, 2020, Art. no. 115892.
- [42] M. J. Islam, Y. Xia, and J. Sattar, "Fast underwater image enhancement for improved visual perception," *IEEE Robot. Autom. Lett.*, vol. 5, no. 2, pp. 3227–3234, Apr. 2020.
- [43] C. Li *et al.*, "An underwater image enhancement benchmark dataset and beyond," *IEEE Trans. Image Process.*, vol. 29, pp. 4376–4389, 2020.
- [44] Y. Wang, J. Guo, H. Gao, and H. Yue, "UIEC $\hat{2}$ -Net: CNN-based underwater image enhancement using two color space," *Signal Process.: Image Commun.*, vol. 96, 2021, Art. no. 116250.
- [45] A. S. A. Ghani and N. A. M. Isa, "Underwater image quality enhancement through integrated color model with Rayleigh distribution," *Appl. Soft Comput.*, vol. 27, pp. 219–230, 2015.
- [46] A. S. A. Ghani and N. A. M. Isa, "Enhancement of low quality underwater image through integrated global and local contrast correction," *Appl. Soft Comput.*, vol. 37, pp. 332–344, 2015.
- [47] A. S. A. Ghani, "Image contrast enhancement using an integration of recursive-overlapped contrast limited adaptive histogram specification and dual-image wavelet fusion for the high visibility of deep underwater image," *Ocean Eng.*, vol. 162, pp. 224–238, 2018.
- [48] X. Fu, P. Zhuang, Y. Huang, Y. Liao, X. Zhang, and X. Ding, "A Retinex-based enhancing approach for single underwater image," in *Proc. IEEE Int. Conf. Image Process.*, 2014, pp. 4572–4576.
- [49] S. Zhang, T. Wang, J. Dong, and H. Yu, "Underwater image enhancement via extended multi-scale Retinex," *Neurocomputing*, vol. 245, pp. 1–9, 2017.
- [50] W. Zhang, L. Dong, X. Pan, J. Zhou, L. Qin, and W. Xu, "Single image defogging based on multi-channel convolutional MSRCR," *IEEE Access*, vol. 7, pp. 72 492–72504, 2019.
- [51] C. Ancuti, C. O. Ancuti, T. Haber, and P. Bekaert, "Enhancing underwater images and videos by fusion," in *Proc. IEEE Conf. Comput. Vis. Pattern Recognit.*, 2012, pp. 81–88.
- [52] C. O. Ancuti, C. Ancuti, C. De Vleeschouwer, and P. Bekaert, "Color balance and fusion for underwater image enhancement," *IEEE Trans. Image Process.*, vol. 27, no. 1, pp. 379–393, Jan. 2018.
- [53] L. Bai, W. Zhang, X. Pan, and C. Zhao, "Underwater image enhancement based on global and local equalization of histogram and dual-image multi-scale fusion," *IEEE Access*, vol. 8, pp. 128973–128990, 2020.
- [54] W. Zhang, X. Pan, X. Xie, L. Li, Z. Wang, and C. Han, "Color correction and adaptive contrast enhancement for underwater image enhancement," *Comput. Electr. Eng.*, vol. 91, 2021, Art. no. 106981.
- [55] W. Zhang, L. Dong, T. Zhang, and W. Xu, "Enhancing underwater image via color correction and bi-interval contrast enhancement," *Signal Process.: Image Commun.*, vol. 90, 2021, Art. no. 116030.
- [56] R. Liu, X. Fan, M. Zhu, M. Hou, and Z. Luo, "Real-world underwater enhancement: Challenges, benchmarks, and solutions under natural light," *IEEE Trans. Circuits Systems Video Technol.*, vol. 30, no. 12, pp. 4861–4875, Dec. 2020.
- [57] T. P. Marques and A. B. Albu, " L^2 UWE: A framework for the efficient enhancement of low-light underwater images using local contrast and multi-scale fusion," in *Proc. IEEE/CVF Conf. Comput. Vis. Pattern Recognt. Workshops*, 2020, pp. 2286–2295.

- [58] C. Li, C. Guo, J. Guo, P. Han, H. Fu, and R. Cong, "PDR-Net: Perception-inspired single image dehazing network with refinement," *IEEE Trans. Multimedia*, vol. 22, no. 3, pp. 704–716, Mar. 2020.
- [59] N. Wang, J. Yu, B. Yang, H. Zheng, and B. Zheng, "Vision-based in situ monitoring of plankton size spectra via a convolutional neural network," *IEEE J. Ocean. Eng.*, vol. 45, no. 2, pp. 511–520, Apr. 2020.
- [60] C. Guo *et al.*, "Zero-reference deep curve estimation for low-light image enhancement," in *Proc. IEEE/CVF Conf. Comput. Vis. Pattern Recognit.*, 2020, pp. 1777–1786.
- [61] X. Xie *et al.*, "Dynamic adaptive residual network for liver CT image segmentation," *Comput. Electr. Eng.*, vol. 91, 2021, Art. no. 107024.
- [62] C. Li, R. Cong, J. Hou, S. Zhang, Y. Qian, and S. Kwong, "Nested network with two-stream pyramid for salient object detection in optical remote sensing images," *IEEE Trans. Geosci. Remote Sens.*, vol. 57, no. 11, pp. 9156–9166, Nov. 2019.
- [63] W. Chao *et al.*, "Discriminative region proposal adversarial network for high-quality image-to-image translation," *Int. J. Comput. Vis.*, vol. 128, pp. 1573–1405, 2020.
- [64] H.-H. Sun, Y. H. Lee, C. Li, L. F. Ow, M. L. M. Yusof, and A. C. Yucel, "The orientation estimation of elongated underground objects via multipolarization aggregation and selection neural network," *IEEE Geosci. Remote Sens. Lett.*, vol. 19, 2022, Art. no. 3505905.
- [65] C. Li, S. Anwar, J. Hou, R. Cong, C. Guo, and W. Ren, "Underwater image enhancement via medium transmission-guided multi-color space embedding," *IEEE Trans. Image Process.*, vol. 30, pp. 4985–5000, 2021.
- [66] Z. Liang, Y. Wang, X. Ding, Z. Mi, and X. Fu, "Single underwater image enhancement by attenuation map guided color correction and detail preserved dehazing," *Neurocomputing*, vol. 425, pp. 160–172, 2021.
- [67] K. Z. M. Azmi, A. S. A. Ghani, Z. M. Yusof, and Z. Ibrahim, "Natural-based underwater image color enhancement through fusion of swarm-intelligence algorithm," *Appl. Soft Comput.*, vol. 85, 2019, Art. no. 105810.
- [68] X. Fu, D. Zeng, Y. Huang, Y. Liao, X. Ding, and J. Paisley, "A fusion-based enhancing method for weakly illuminated images," *Signal Process.*, vol. 129, pp. 82–96, 2016.
- [69] S. Wang, K. Ma, H. Yeganeh, Z. Wang, and W. Lin, "A patch-structure representation method for quality assessment of contrast changed images," *IEEE Signal Process. Lett.*, vol. 22, no. 12, pp. 2387–2390, Dec. 2015.
- [70] K. Panetta, C. Gao, and S. Agaian, "Human-visual-system-inspired underwater image quality measures," *IEEE J. Ocean. Eng.*, vol. 41, no. 3, pp. 541–551, Jul. 2016.
- [71] C. Li *et al.*, "ASIF-Net: Attention steered interweave fusion network for RGB-D salient object detection," *IEEE Trans. Cybern.*, vol. 51, no. 1, pp. 88–10, Jan. 2021.
- [72] G. Ferri, A. Munaf, and K. D. LePage, "An autonomous underwater vehicle data-driven control strategy for target tracking," *IEEE J. Ocean. Eng.*, vol. 43, no. 2, pp. 323–343, Apr. 2018.
- [73] M. Sun, Z. Gu, H. Zheng, B. Zheng, and J. Watson, "Underwater wide-area layered light field for underwater detection," *IEEE Access*, vol. 6, pp. 63 915–63922, 2018.
- [74] C. Li, C. Guo, and C. L. Chen, "Learning to enhance low-light image via zero-reference deep curve estimation," *IEEE Trans. Pattern Anal. Mach. Intell.*, early access, 2021, doi: [10.1109/TPAMI.2021.3063604](https://doi.org/10.1109/TPAMI.2021.3063604).
- [75] M. Ju, C. Ding, W. Ren, Y. Yang, D. Zhang, and Y. J. Guo, "IDE: Image dehazing and exposure using an enhanced atmospheric scattering model," *IEEE Trans. Image Process.*, vol. 30, pp. 2180–2192, 2021.



Weidong Zhang (Graduate Student Member, IEEE) is working toward the Ph.D. degree in information and communication engineering with the School of Information Science and Technology, Dalian Maritime University, Dalian, China.

He is also a Teaching Assistant with the School of Information Engineering, Henan Institute of Science and Technology, Xinxiang, China. His current research interests include image processing, computer vision, and machine learning.



Yudong Wang is working toward the Ph.D. degree in information and communication engineering with the School of Electrical and Information Engineering, Tianjin University, Tianjin, China.

His current research interests include image processing, computer vision, and deep learning, particularly in the domains of image restoration and enhancement, such as images captured under the bad weather (hazy, foggy, etc.) and special circumstances (especially underwater). His research interests also focus on other high-level vision problems, such as object detection, salient object detection, etc.



Chongyi Li received the Ph.D. degree in information and communication engineering from the School of Electrical and Information Engineering, Tianjin University, Tianjin, China, in 2018.

From 2016 to 2017, he was a Joint-Training Ph.D. Student with the Australian National University, Canberra ACT, Australia. He was a Postdoctoral Research Fellow with the Department of Computer Science, City University of Hong Kong, Hong Kong. He is currently a Research Assistance Professor with the School of Computer Science and Engineering,

Nanyang Technological University, Singapore, Nanyang Technological University, Singapore. His current research interests include image processing, computer vision, and deep learning, particularly in the domains of image restoration and enhancement.